DESIGN AND MODELING OF THE DYNAMIC UNDERACTUATED FLYING-WALKING (DUCK) ROBOT

by

Christopher J. Pratt

A Thesis submitted to the faculty of
The University of Utah
in partial fulfillment of the requirements for the degree of

Master of Science

Department of Mechanical Engineering

The University of Utah

January 2017

The University of Utah Graduate School

STATEMENT OF DISSERTATION APPROVAL

The dissertation of **Christopher J. Pratt**
has been approved by the following supervisory committee members:

Kam K. Leang ,	Chair(s)	**12/28/2016** Date Approved
Sanford G. Meek ,	Member	**12/7/2016** Date Approved
Tucker Hermans ,	Member	**12/7/2016** Date Approved

by **Tim Ameel** , Chair of
the Department of **Mechanical Engineering**
and by **David B. Kieda** , Dean of The Graduate School.

ABSTRACT

This thesis focuses on the design, modeling, fabrication, and testing of a flying and walking robot, called the dynamic underactuated flying-walking (DUCK) robot. The DUCK robot combines a high-mobility flying platform, such as a quadcopter (quadrotor helicopter), with passive-dynamic legs to create a versatile system that can fly and walk. One of the advantages of using passive-dynamic legs for walking is that additional actuators are not needed for terrestrial locomotion, therefore simplifying the design, reducing overall weight, and decreasing power consumption. First, a mathematical model is developed for the DUCK robot, where the modeling combines the passive-dynamic walking mechanism with the swinging mass of the aerial platform. Second, simulations based on the model are used to help guide the design of two prototype robots, specifically to tailor the shape of the feet and the dimensions of the passive-dynamic walking mechanism. Third, an energy analysis is performed to compare the performances between flying and walking. More specifically, simulation results show that continuous active walking has a comparable energy efficiency to that of flying for the two prototype designs. For design Version 1, it is estimated that the robot is able to walk up to 1600 meters on a 30kJ battery (standard Li-Po battery) with a cost of transport of 1.0, while the robot can potentially fly up to 1800 meters horizontally with the weight of its legs and up to 2300 meters without the weight of its legs. Design Version 2 is estimated to be able to walk up to 4600 meters on a 30kJ battery with a cost of transport of .50, while it could fly up to 2600 meters with the weight of its legs or 4300 meters without its legs. The cost of transport of flying is estimated to be .89 in all scenarios. Finally, experimental results demonstrate the feasibility of combining an aerial platform with passive-dynamic legs to create an effective flying and walking robot. Two modes of walking are experimentally demonstrated: (1) passive walking down inclined surfaces for low-energy terrestrial locomotion and (2) active (powered) walking leveraging the capabilities of the flying platform, where thrust from the quadcopter's rotors enables the DUCK robot to walk on flat surfaces or up inclined surfaces.

CONTENTS

ABSTRACT . . . . . **iii**

LIST OF FIGURES . . . . . **vi**

LIST OF TABLES . . . . . **ix**

NOTATION AND SYMBOLS . . . . . **x**

ACKNOWLEDGEMENTS . . . . . **xi**

CHAPTERS

1. INTRODUCTION **1**

1.1 Background and Motivation 1
1.2 Research Objectives and Contributions 2
1.3 Summary of Achievements 3
1.4 Organization 3

2. BACKGROUND AND STATE-OF-THE-ART **4**

2.1 Aerial Terrestrial Robots 4
2.2 Passive Dynamic Walking 5
2.3 Modeling and Simulation of Passive Dynamic Walking 8
2.4 Knowledge Gaps in Passive Dynamic Walking 10

3. DYNAMICS MODELING **13**

3.1 Flying-Walking Robot Concept 13
3.2 Dynamics Modeling 15
3.2.1 The Equations of Motion 15
3.2.2 Handling Collisions 20

4. SIMULATION, DESIGN, AND PROTOTYPE DEVELOPMENT **23**

4.1 DUCK Robot Designs 23
4.2 Prototype Manufacturing: Version 1 24
4.3 Prototype Manufacturing: Version 2 25

5. PERFORMANCE CHARACTERIZATION AND ENERGY ANALYSIS **27**

5.1 Performance of Version 1 Design 27
5.1.1 Active Walking 28
5.1.2 Flying 30
5.2 Performance of Version 2 Design 30
5.3 Energy Analysis 32

6. CONCLUSIONS **38**

REFERENCES **40**

LIST OF FIGURES

1.1 Examples of passive dynamic walkers [3]. 1

1.2 Prototypes of the DUCK robot: (a) Version 1 and (b) Version 2. The flying platform in (a) is a commercially available Iris (3D Robotics) quadcopter [25]. The flying platform in (b) is custom-designed. The feet in both designs are 3D-printed from ABS material, then treated with acetone for smoothness. Hip joints consist of a shaft and ball bearings. 2

2.1 Concept of a passive-dynamic walker [29]: (a) The mechanism oscillates the leg and feet side-to-side, where each foot makes contact with the ground surface as shown. (b) While the front leg is in contact with the ground the back leg swings forward, taking a step. This cycle continues indefinitely on a sloped surface. 6

2.2 Examples of a walker with curved feed [30]: (a) shows a front (lateral view of the mechanism and (b) show a side (sagittal) view. Note how the mechanism is kept stable by placing the center of gravity below the foot's center of curvature (denoted by R_f and R_s). 6

2.3 Non-bipedal walkers: (a) is a four legged active walker, which has a passive-dynamic walker design powered by a servo controlled swinging mass [17], (b) is a many legged, laterally rocking, walker [28], and (c) is a four legged walker not reliant on lateral rocking [21]. 9

2.4 Examples of running robots: (a) is a passive-dynamic walker capable of running. The ankle springs make the mechanism "jump" and become airborne as the feet transition [22]; and (b) is a highly mobile powered "cheetah" robot capable of running, jumping, and traversing uneven terrain [27]. 12

3.1 The modes of operation for the proposed passive-dynamic flying-walking DUCK robot, showing (a) flying mode, then transitioning to (b) passive walking mode, followed by flying again, and finally, (c) active (powered) mode where the quadcopter's rotors provide the needed force to enable the robot to take steps and walk on flat or up inclined surfaces. 14

3.2 Key features of the DUCK robot: (a) key components of the robot, (b) illustration of passive walking without power down a slope of angle ϕ, and (c) illustration of active (powered) walking on flat ground or up a slope of angle γ. During active walking rear thrusters provide forward thrust and rocking motion to enable the robot to take steps and walk. 16

3.3 Depiction of how the 3D walking motion is split into separate lateral and sagittal motions for modeling [14]–[16]. (a) shows the 3D motion projected onto the 2D lateral and sagittal planes. (b) and (c) are free body diagrams for the lateral and sagittal motions, respectively. Forces ($\vec{F}_{...}$) are determined independently during simulation. 22

3.4 Outline of dimensions used in the DUCK robot. (a) The lateral dimensions and (b) the sagittal dimensions. 22

4.1 Simulated phase portrait for the left leg of Version 1 of the DUCK robot, showing the robot beginning to enter a stable limit cycle. The robot was started from rest standing straight up with θ_{2L} (lateral lean) = 2.3° and ϕ (slope angle) = -2.3°. No thruster forces were used. 24

4.2 Mechanical drawings of the passive-dynamic walking legs, comparing Version 1 (left) and Version 2 (right) designs, where (a) and (c) show the dimensions and (b) and (d) show an exploded view of the mechanism. 26

5.1 Experimental setup for testing passive-dynamic walking. The DUCK robot's position is recorded by a Vicon motion capture system while it walks down the sloped treadmill. Cameras are the Vicon MX F20 and MX T160 series running at 100 Hz, treadmill is a Cadence 70e series. Here ϕ (slope angle) = -2.3°. 28

5.2 Comparison of experimental and simulated results of the robot passively walking. The DUCK robot was allowed to reach a steady walking state on the treadmill shown in **Figure 5.1** while having its position recorded by a motion capture system. An starting point was chosen from this data and used to define the initial state in the simulation. Sagittal quadcopter angle, the angle of joint 3 in **Figure 3.3**(c), is θ_{3S} and lateral lean angle, the angle of joint 2 in **Figure 3.3**(b), is θ_{2L}. Here ϕ (slope angle) is -2.3°. 29

5.3 Sequence shots of Version 1 of the DUCK robot flying, walking, and then flying again: (a) flying, (b) active (powered) walking on flat surface, (c) passive walking with motors turned off down a -3.1° slope, (d) active walking up a 2.7° slope, and finally (e) take off and flight. 30

5.4 Second experimental setup for testing passive-dynamic walking. Like the previous test the DUCK robot's position is recorded by a Vicon motion capture system while it walks down the sloped treadmill. Cameras are the Vicon MX F20 and MX T160 series running at 100 Hz, treadmill is a Cadence 70e series. Here (slope angle) = -2.3. 31

5.5 Comparison of experimental results of Version 2 of the robot with (a) raw simulated results and (b) altered simulated results, of the DUCK robot's joint angles as it passively walks down a -2.3° slope. In (b) the simulation's lateral moment of inertia was altered so the frequency of the simulated θ_{2L} matched the real data as a demonstration of the system's dependency on the lateral rocking frequency. 33

5.6 Free body diagram of flying. Depicted are the forces and velocities used for calculating the energy efficiency of flying. 33

5.7 Example thruster pattern used for active walking in the simulation. The pattern follows the repetitive motion of θ_{2L}. The rear thrusters are used to provide forward thrust and alter the walking frequency. 35

5.8 Simulation result of estimated maximum distance traveled on 30 kJ (energy in a 2.5 Ah, 11.1 volt battery) v.s. speed for flying and walking. Results for the Version 1 of the DUCK robot are shown in (a), and results for Version 2 are shown in (b). Both version have limits for how fast they can walk without falling over. 36

5.9 Simulation result of the cost of transport for flying and walking. Results for the Version 1 of the DUCK robot are shown in (a), and results for Version 2 are shown in (b). Active walking for Version 1 and 2 has a cost of transport of 1.0 and .50 respectively. Flying has a cost of transport of .89. 36

LIST OF TABLES

3.1 Newton-Euler joints for the lateral motion 19
3.2 Applied thruster and frictional forces for the lateral motion 19
3.3 Torsional friction for the lateral motion 19
3.4 Newton-Euler joints for the sagittal motion 20
3.5 Applied thruster and frictional forces for the sagittal motion 20
3.6 Torsional friction for the sagittal motion 20

NOTATION AND SYMBOLS

$\times$	cross product
$\bullet$	dot product
a, A	scalars
$\vec{a}$, $\vec{A}$	vectors
$\hat{x}$,$\hat{y}$,$\hat{z}$	unit vectors
$\vec{A}_{i\{j\}}$	vector $\vec{A}_i$ projected onto axis j
$\mathbf{A}$, $\boldsymbol{B}$	matrices
$E_{qu,i}$	equation describing the forces or torques on joint i
m_i	mass of link i
N	number of joints
$\vec{g}$	gravity
θ_i, $\dot{\theta}_i$, $\ddot{\theta}_i$	scalar angular position, velocity, and acceleration and joint i relative to the inertial axis
$\vec{\omega}_i$, $\dot{\vec{\omega}}_i$	vector angular velocity and acceleration of joint i, relative to the inertial axis
$\vec{d}_i$, $\dot{\vec{d}}_i$, $\ddot{\vec{d}}_i$	linear distance, velocity, and acceleration from joint $i-1$ to joint i
$\vec{F}_{applied,i}$	an applied force on link i
$\vec{d}_{\vec{F}_{applied,i}}$	linear distance from the center of gravity of link i to $\vec{F}_{applied,i}$
$\dot{\vec{v}}_i$	linear acceleration of joint i relative to the inertial axis
$\dot{\vec{v}}_{cg,i}$	linear acceleration of joint i's center of gravity relative to the inertial axis
$\vec{u}_{Fric,i}$	torsional friction on joint i
$\vec{F}_i$	total force on link i
$\vec{u}_i$	total torque on joint i
$\mathbf{R}_{i,j}$	rotation matrix to change the reference axis of a vector from axes i to axes j

ACKNOWLEDGEMENTS

First, I express my sincere gratitude and appreciation to my advisor, Kam K. Leang, for his expert guidance, encouragement, and mentorship.

Second, I thank Profs. Sanford Meek and Tucker Hermans for being on my committee and providing input on my work.

Next, I gratefully acknowledge the research support from the National Science Foundation, Partnership for Innovation Program, Grant No. 1430328.

Finally, this project would have never been completed without the encouragement and devotion of my family and friends. In particular, I thank my parents for their constant love, patience, and support. I also thank my lab mates from the DARC Lab, for their support and the laughs.

CHAPTER 1

INTRODUCTION

This work describes the design, modeling, development, and feasibility testing of a flying and walking robot, called the Dynamic Underactuated Flying-Walking (DUCK) robot. The DUCK robot combines a high-mobility flying platform, such as a quadcopter (quadrotor helicopter), with passive-dynamic legs (**Figure 1.1**) to create a versatile system that can fly and walk. Two prototype DUCK robots, referred to as Version 1 and Version 2, shown in **Figure 1.2** were developed and tested. The main goal of this work is to explore a new way of adding a light weight and low energy form of ground locomotion to a flying robot to broaden the application of aerial robotic platforms.

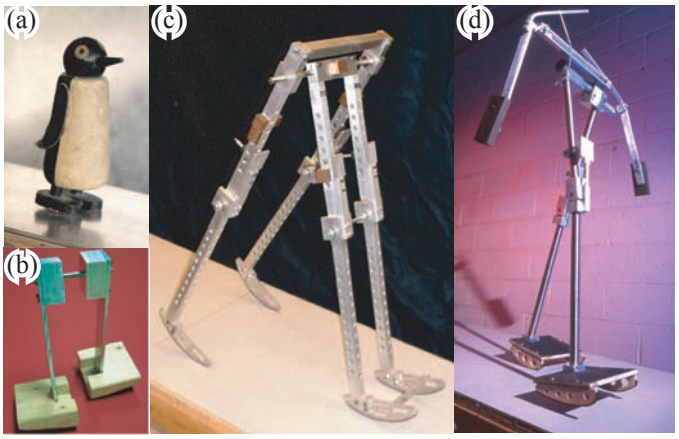

Figure 1.1: Examples of passive dynamic walkers [3].

1.1 Background and Motivation

In the last decade a lot of effort has gone into research on aerial robots, such as quadcopters. Quadcopters are a attractive research platform as they offer high mobility and versatility at a relatively low cost. However, one of their biggest challenges is their high energy consumption and limited ability to carry weight/fuel. This limits a quadcopter's

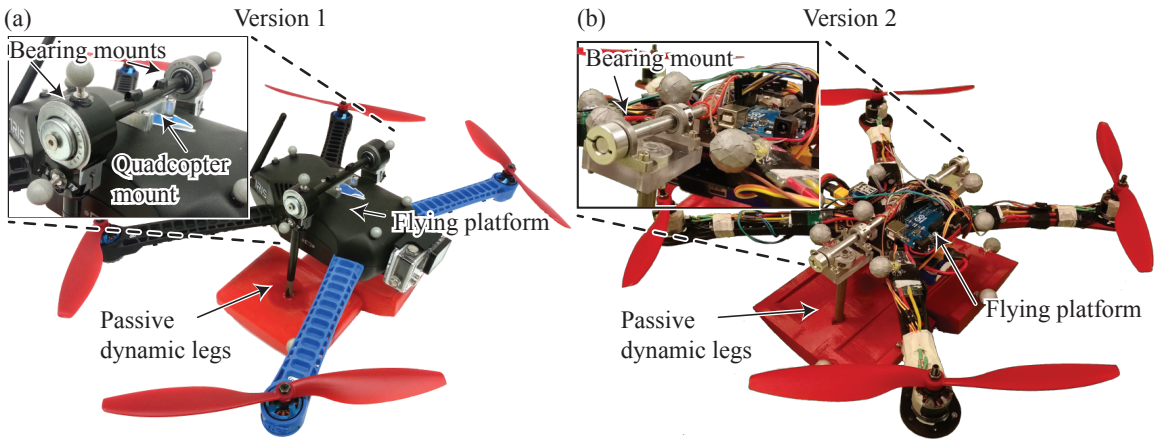

Figure 1.2: Prototypes of the DUCK robot: (a) Version 1 and (b) Version 2. The flying platform in (a) is a commercially available Iris (3D Robotics) quadcopter [25]. The flying platform in (b) is custom-designed. The feet in both designs are 3D-printed from ABS material, then treated with acetone for smoothness. Hip joints consist of a shaft and ball bearings.

operation time, especially when carrying a heavy payload. Recently, some attention has focused on developing flying robots with the ability to walk, swim, roll, etc., to enhance the robot's versatility and/or offer energy-efficient modes of travel to supplement high-energy flight [15]. Such designs have advantages in situations where the robot may need to fly to overcome large obstacles, yet have the ability to slowly traverse terrain and operate over a long period of time.

There have been many successful attempts to create robots with aerial and terrestrial locomotive capabilities. The designs for such robots include things such as powered legs [33], motorized wheels [18], or circular rolling exoskeletons [16]. Although effective, many of these designs require additional actuators for ground locomotion. Adding actuators increases weight and design complexity, which increases power consumption, especially during flight. The flying-walking DUCK robot design described in this thesis uses passive-dynamic walking legs to achieve ground locomotion, which requires no additional actuators to function, resulting in a lighter and simpler robot.

1.2 Research Objectives and Contributions

This thesis has three objectives. The first is to introduce a new, lightweight, and energy efficient design, which combines a quadcopter with passive-dynamic walking legs, to create an aerial-terrestrial robot which can fly and walk. The second objective is to model

the dynamics of the robot for use in the design of the key components of the walking mechanism. Finally, the third objective is to determine through simulation if such a aerial-terrestrial robot has any energy efficiency advantages over a purely flying robot. Both simulation and experimental results are compared. Thus, the contributions of this thesis includes: (1) developing a mathematical model of the DUCK robot's walking and flying characteristics, (2) exploiting the robot's model and simulations to guide the design of two prototype robots, (3) analyzing the energy consumption for flying versus walking, and (4) comparing the model with physical experiments for the two different robot designs.

1.3 Summary of Achievements

This work resulted in a new functional design of an aerial-terrestrial robot which combines a quadcopter with passive-dynamic walking legs. This project leveraged previous works on the design and modeling of passive-dynamic walkers [29–31] to create a mathematical model to guide the design of the flying-walking robot. A method to handle collisions for the passive-dynamic walker during the walking motion is presented. A simulation based on the model is then used to design two different prototype DUCK robots. Simulation and experimental results are compared, where two different validations are performed, one with the first DUCK robot and one with a higher tolerance DUCK robot design. Lastly, an energy analysis is performed to compare how far both robots could walk versus fly on the same battery charge. In this case, actuator disk theory is used to place a theoretical maximum on the efficiency of the quadcopter's propellers. This work resulted in a published conference proceedings entitled, "Dynamic Underactuated Flying-Walking (DUCK) Robot", IEEE Int. Conf. on Robotics and Automation (ICRA), pages 3267-3274, May 16-21, 2016, Stockholm Waterfront Congress Centre, Sweden [25].

1.4 Organization

This thesis is organized as follows. First, a detailed background is presented in Chapter 2, followed by the dynamics modeling of the DUCK robot in Chapter 3. In Chapter 4, simulation, design, and prototype manufacturing is presented. In Chapter 5, the performance characterization and energy analysis are presented. Finally, conclusions are presented in Chapter 6.

CHAPTER 2

BACKGROUND AND STATE-OF-THE-ART

2.1 Aerial Terrestrial Robots

Research into supplementing flying robots with forms of ground locomotion has recently gained interest in the robotics community. Though there has been intermittent work in air/land robots, the majority of the work in this field started in 2010 [18]. The work in this field aims to increase the versatility and/or energy efficiency of the supplemented flying robot. The field has yet to converge on a general robot design which research aims to iterate on and improve upon. Instead a wide variation of successful and very experimental robots has emerged employing a large variety of designs. For example, some robots use a quadcopter platform attached to a ground locomotive device. Robots like this include the Multi-Tentacle Air Vehicle [33]. This design features a quadcopter with three limbs made of servo actuated joints that can walk, perch, and grasp. Another robot developed by Kalantari uses a quadcopter with shape memory allow actuated feet [14]. The MMAR's flying platform has servo actuated legs tipped with free-spinning wheels which can be locked to cycle between rolling and walking [6]. Other robots use motor powered wheels, such as the one designed by Elsamanty [8]. Elsamanty's robot has four motorized wheels, two omnidirectional and two regular, enabling the robot to drive along the ground. Still other robots use quadcopters inside rolling cages, such as HyTAQ and the robot designed by Dudley which use a cage that freely spins about the pitch axis [7, 15], or MUWA which rolls on a fixed disk about the yaw axis [16]. These cage designs are unique in that they leverage the propulsive mechanism of the robot.

Research into air/land robots is not just limited to quadcopters. There are robots which use insect inspired legs and wings such as BOLT and DASH [23, 24]. These robots can operate in either a purely legged walk, a wing assisted walk, or a flying mode. Bozkurt

even made a biorobot from a living moth by controlling its leg and wing muscles through implanted electrodes [2]. Other designs use propeller driven planes outfitted with a form of crawling, such as the MMALV [1] which crawls on wheel-legs. Daler has also created two robots with similar forms of locomotion, but are unique in that the robot crawls by rotating its wings [4, 5].

Although effective, many of these designs require additional actuators for ground locomotion. Adding actuators increases weight and design complexity, which increases power consumption, especially during flight. The robot design described in this thesis presents a new way of enabling ground locomotion to a flying robot through the addition of passive-dynamic walking legs. This approach requires no additional actuators to function, resulting in a relatively low-power, low-weight system with added versatility.

2.2 Passive Dynamic Walking

Between 1988 and 1993, Tad McGeer introduced the concept of a passive-dynamic walker to the scientific community [20]. A passive-dynamic walker is "a simple mechanical device, composed of solid parts connected by joints, which walks stably down a slope" [3]. Put differently, they are mechanisms lacking actuators and control systems which use the force of their own weight to walk down a slope. An example of such a mechanism is pictured in **Figure 2.1**. There are two main reasons for their interest in the scientific community. First, they are incredibly simple compared to their walking robotic counterparts that involve actuators and other motion-creating mechanisms [26, 27]. A passive-dynamic walker is mechanically simple as it requires no actuators to function, and is simple to control as it must be passively stable. Second, passive walkers are inherently low energy since they must operate on only their own potential energy. By contrast, powered (active) walking robots are often more complex and consume more power.

To date, essentially all the designs for passive-dynamic walking mechanisms use effectively two sets of legs. At any given moment one set supports the device while the other set steps forward. When placed on the correct slope with the right initial conditions, the mechanism naturally oscillates, alternating the legs between the roles of supporting the mechanism and stepping forward. The energy of the mechanism's mass moving down the slope is used to counteract losses due to sources such as friction and collisions, creating

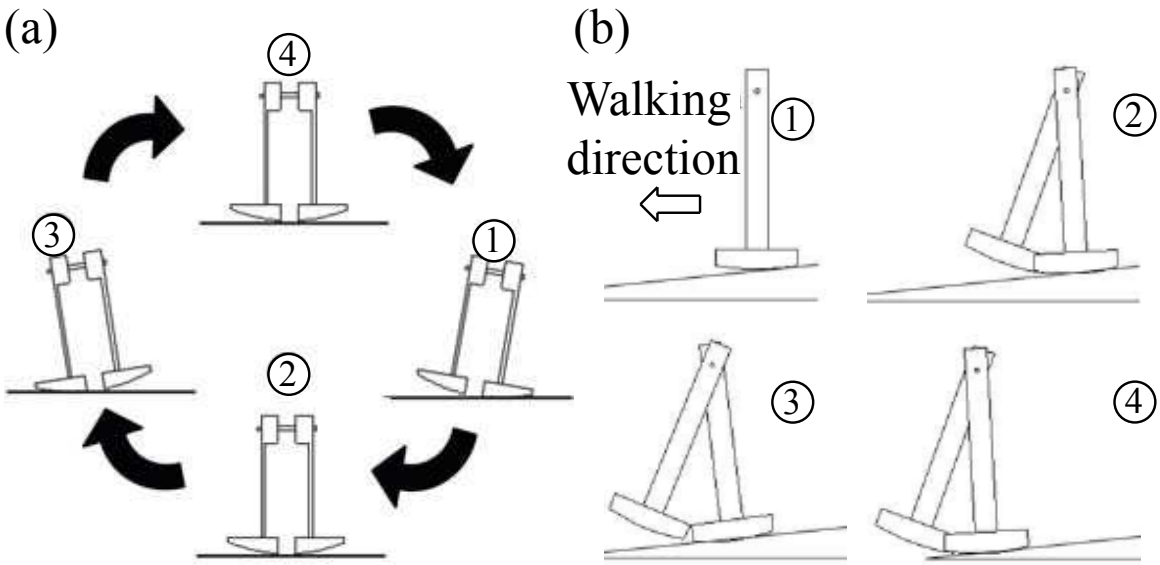

Figure 2.1: Concept of a passive-dynamic walker [29]: (a) The mechanism oscillates the leg and feet side-to-side, where each foot makes contact with the ground surface as shown. (b) While the front leg is in contact with the ground the back leg swings forward, taking a step. This cycle continues indefinitely on a sloped surface.

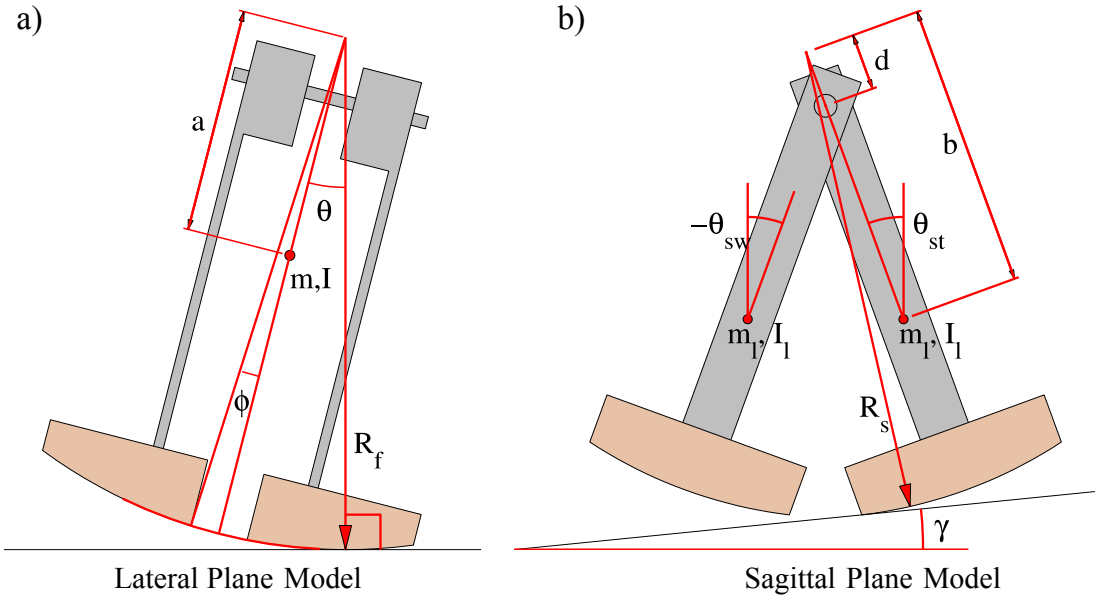

Figure 2.2: Examples of a walker with curved feed [30]: (a) shows a front (lateral view of the mechanism and (b) show a side (sagittal) view. Note how the mechanism is kept stable by placing the center of gravity below the foot's center of curvature (denoted by R_f and R_s).

a self-sustaining walk. The mechanism will stop walking when it reaches the end of the sloped surface, or when it meets a disturbance that places it outside the bounds of its stable walking motion.

At the current state of research there are two basic designs for walkers, ”2D” and ”3D” walkers. 3D walkers are distinguished by their large curved feet, as pictured in **Figure 2.1** and **Figure 1.1** (a) and (b). This design is discussed in [12, 28, 30]. The feet form a sphere-like shape with a center of curvature at or above the mechanism's center of mass, as shown in **Figure 2.2**. This forms a base which is naturally stable, and causes the system to oscillate when perturbed. If oscillated laterally (shoulder-to-shoulder) the rocking will alternate which foot is in contact with the ground, as illustrated in **Figure 2.1**(a). If this oscillation happens on a slope then sagittal (front-to-back) motion will occur where the non-grounded leg swings forward under the force of its own weight. If the mechanism's lateral oscillation happens at the right frequency such that the free swinging leg reaches the apex of its swing as the foot touching the ground transitions, the mechanism will enter a self sustaining passive-dynamic walk, as illustrated in **Figure 2.1**. Ideally this process will continue indefinitely until the walker reaches the end of its slope, or is met with some outside disturbance.

The 2D walker design is pictured in **Figure 1.1**(c). This design is described in detail in [13, 32]. These walkers have two rigidly connected inner legs and two rigidly connected outer legs. Their feet are usually a one (instead of two) dimensional curve with a smaller radius, and they do not employ lateral rocking. Instead, one pair of legs supports the device while the other pair swings forward under the force of its own weight. To keep the swinging leg from prematurely hitting the ground the mechanism usually has knees. The design is such that the grounded leg will stay fully extended while the free swinging leg is slightly bent, making it effectively shorter. When the swinging leg reaches the apex of its motion it naturally extends its knee and hits a mechanical stop. The mechanism then leans forward, and the previously grounded leg bends at the knee, completing one cycle. Again, this process ideally continues indefinitely until the walker is met with some external disturbance.

Since 1988, the most simple passive-walker designs have been thoroughly explored. This includes the mathematical modeling [10], construction and testing [30], and slight

deviations from traditional designs [3]. In 1999, researchers began branching out into possible applications and more complicated designs of passive-dynamic walkers. However, the field can still be considered in its infancy, and has yet to be worked into many practical applications.

One such branch of passive-dynamic walking is four-legged (or more) walkers, such as the ones pictured in **Figure 2.3**. Such walkers are usually multiple instances of their simpler counterparts connected together. Examples of this are shown in **Figure 2.3**(a) and (b), which are multiple instances of the rocking walker shown in **Figure 2.1** connected together. Such designs are beneficial as they are inherently more stable then their bipedal counterparts. Another branch of research is walkers with increased complexity. An example is pictured in **Figure 1.1**(d), which uses a combination of legs with knees, lateral oscillation, and passively balancing arms. This device achieves a slightly more robust walk than either of the two basic designs on their own. Perhaps the most impressive example of a complex passive-dynamic walker to date is the passive-dynamic runner shown in **Figure 2.4**(a). This mechanism is a 2D passive-dynamic walker with ankles containing a linear slide connected to a spring. This literally "puts a spring in its step" and allows the walker to run, where the mechanism is airborne during the transition between each foot.

A growing branch of passive-dynamic walking is active/quasi-passive walking. These walking robots add active elements to passive designs. This usually includes either indirect powering of a 3D walker's legs (active walking) or active control of the walker's passive dynamics (quasi-passive walking). These robots use mechanisms like actuated ankles [30], or active springs [32] to power the robot. The work in this thesis builds upon the idea of a active 3D walker by creating a robot which powers its passive-dynamic legs using the thrust of a quadcopter. Additionally, most passive-dynamic walker designs vary the mass and size of the robot to create a stable passive walking motion. However in this work there are strict limits on the size and weight of the walker to ensure the robot can still fly. Thus stabilization was done without relying on those commonly used parameters.

2.3 Modeling and Simulation of Passive Dynamic Walking

Regardless of design, all passive walkers require intensive tuning of their passive dynamics to become effective walkers. The majority of the efforts to create operational pas-

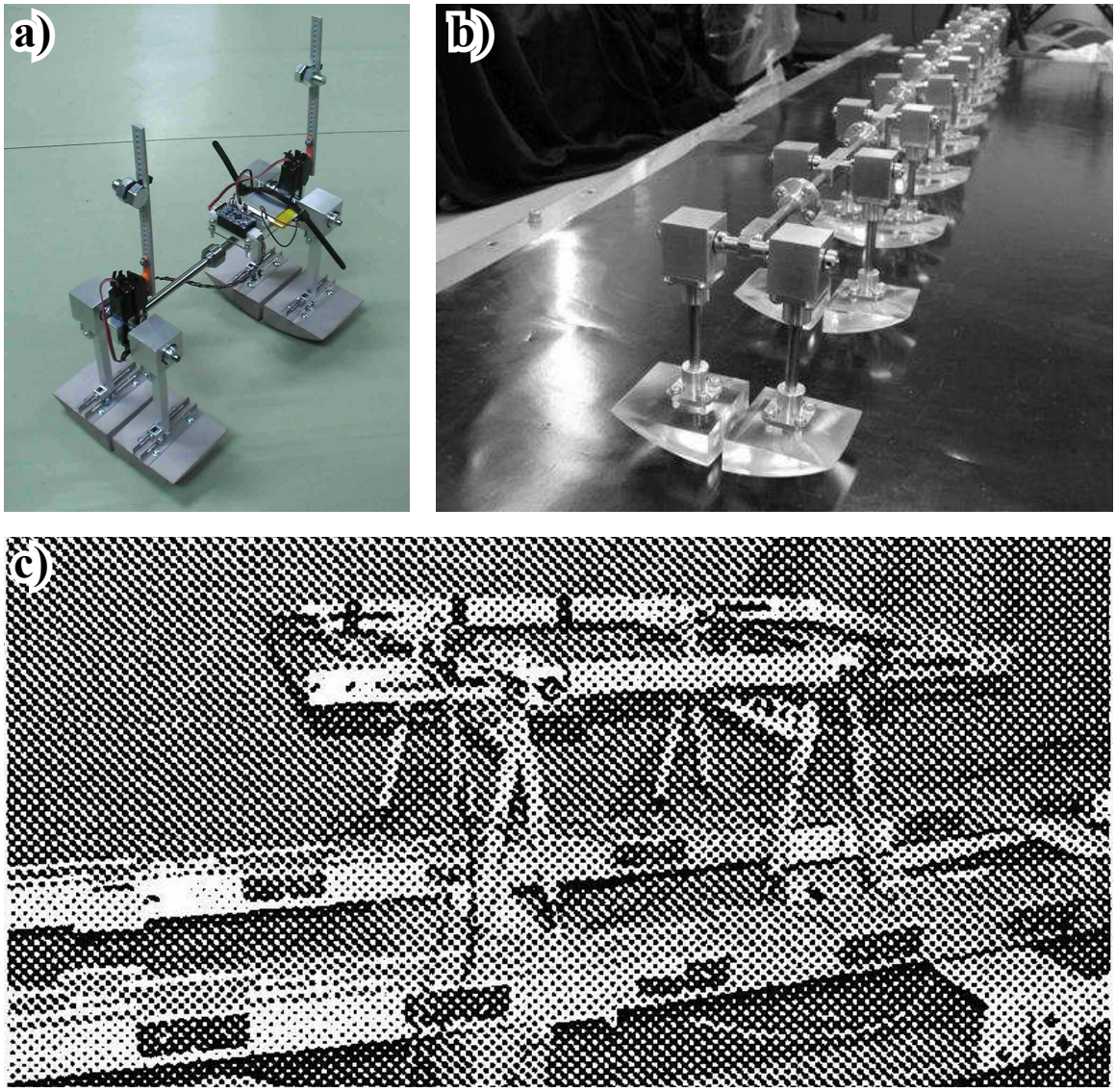

Figure 2.3: Non-bipedal walkers: (a) is a four legged active walker, which has a passive-dynamic walker design powered by a servo controlled swinging mass [17], (b) is a many legged, laterally rocking, walker [28], and (c) is a four legged walker not reliant on lateral rocking [21].

sive walkers rely on modeling and computer simulation [9, 11, 19]. However, most researchers do not model the true 3D motion of the walker, and instead break it down into two 2D components. Additionally, walkers such as the one pictured in **Figure 1.1**(c) are considered to be purely 2D and are modeled with only the motion in the sagittal (front-to-back) plane. The 2D motion is described by adapting the well known equations for a walker of this sort presented in [10], which takes the form

$$\mathbf{M}(\vec{\theta}_j)\ddot{\vec{\theta}}_j + \mathbf{H}(\vec{\theta}_j, \dot{\vec{\theta}}_j)\dot{\vec{\theta}}_j + \mathbf{G}(\vec{\theta}_j, \vec{\theta}_s) = 0, \tag{2.1}$$

where **M**, **H**, and **G** are matrices describing the inertial, Coriolis, and gravitation forces on each joint, respectively; $\vec{\theta}_j$, $\dot{\vec{\theta}}_j$, and $\ddot{\vec{\theta}}_j$, are vectors containing each joint's angular position, velocity, and acceleration, respectively; and $\vec{\theta}_s$ is the angle of the slope. The equation of motion is used to solve for $\ddot{\vec{\theta}}_j$, which then can be used to simulate the walker through numerical integration. The equations for the collision which occurs when the knees lock or the feet hit the ground are solved using the conservation of angular momentum.

Papers using a 3D walker such as the one depicted in **Figure 1.1**(b) break the 3D motion of the walker into two 2D descriptions of the motions in the lateral and sagittal planes [30]. This requires two equations like **Equation 2.1**, as well as two equations describing collisions in both planes. In this method the lateral and sagittal equations are completely decoupled except collisions are assumed to happen at the same time in both planes.

2.4 Knowledge Gaps in Passive Dynamic Walking

Though passive walking is a interesting and well-researched field, there is still much research that remains to be done and problems to be solved. Though opinions may vary, the end goal of research on legged locomotion is to create robust walking robots. Walking, as a form of locomotion, has many attractive features such as its ability to traverse a wide range of terrains. Passive-dynamic walking is still far away from reaching this goal. Current mechanisms have the energy efficiency required for many applications, but lack the needed robustness and practicality. Currently, in order to function walkers need to be placed in the correct scenario with the right initial conditions (a flat, smooth, 4° - 10° slope with the right joint positions). Once walking starts, unexpected disturbances, such as an outside push or accidental foot scuffing, causes the walker to fail. Even after a sustainable gait is established, over time the dynamics can come out of phase, again causing the walker

to fail. Thus the knowledge gap lies mostly in the creation of a walker which is robustly stable in a wide range of situations. Once walkers are created that are more robustly stable, they will be applicable in situations with more inherent instability. There is already a push to create walkers like this, such as the creation of active-dynamic walkers, or walkers that use more stable flat feet with ankles in place of curved feet [11, 31]. This is still only a start, however, and further investigation is required before all the current problems are overcome.

There is also a knowledge gap in the math used to model the passive-dynamic walking. The gap mostly lies in decoupling of the lateral and sagittal motions. This simplification especially effects 3D walkers, whose lateral and saggital movements are continuously interacting with each other. Additionally, solving collisions between the feet and the ground with the conservation of angular momentum does not accurately describe the energy lost as the walker's feet scuff the ground, which is one of its two main forms of energy loss.

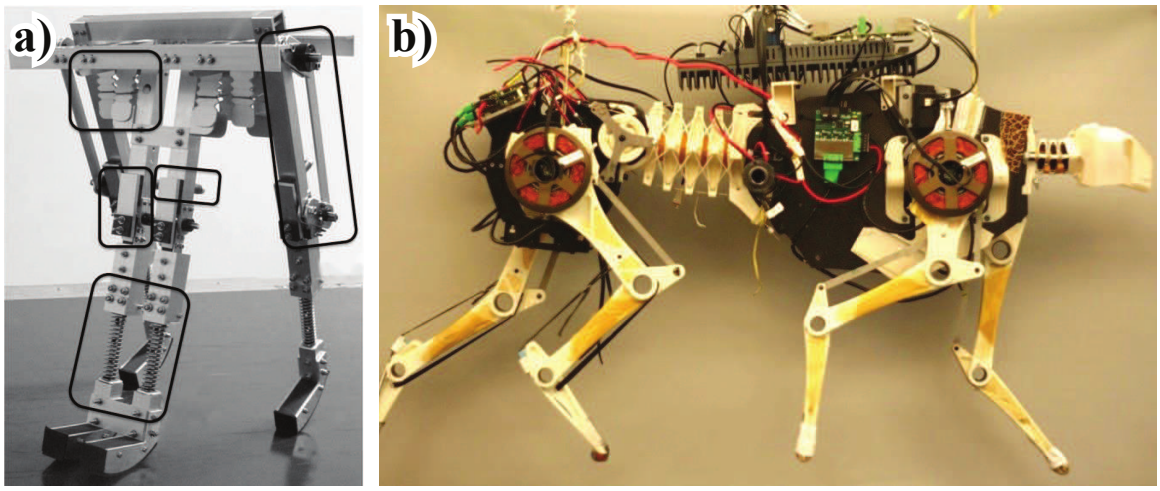

Figure 2.4: Examples of running robots: (a) is a passive-dynamic walker capable of running. The ankle springs make the mechanism "jump" and become airborne as the feet transition [22]; and (b) is a highly mobile powered "cheetah" robot capable of running, jumping, and traversing uneven terrain [27].

CHAPTER 3

DYNAMICS MODELING

3.1 Flying-Walking Robot Concept

The remainder of this thesis describes the development of the dynamic underactuated flying-walking (DUCK) robot. The DUCK robot is created by combining a multi-rotor aerial platform (such as a quad-rotor helicopter or quadcopter) with passive-dynamic legs, is capable of both aerial and terrestrial locomotion. Recently, some attention has focused on developing aerial robots with the ability to walk, swim, roll, etc., to enhance versatility and/or offer energy-efficient modes of travel to supplement high-energy and high-mobility flight [15]. Such designs have advantages in situations where the robot may need to fly to overcome large obstacles, yet have the ability to slowly traverse terrain and operate over a long period of time. As depicted in **Figure 3.1**, the proposed DUCK robot has three basic modes of operation: (a) flying in situations that demand it, (b) low-energy passive walking down inclined surfaces (motors turned off), and (c) active (powered) walking where the quadcopter's rotors provide the needed forces to enable the robot to take steps and walk on flat, or up inclined, surfaces. The contributions of this work include: (1) mathematical modeling of the DUCK robot; (2) design of the robot through simulation; (3) creation of a prototype to demonstrate flying and passive/active walking; and (4) an energy analysis to compare the power consumption of flight to that of active walking.

Herein, a passive walking mechanism is combined with a quadcopter flying platform to create an aerial terrestrial robot (ATR). The resulting ATR can both walk using the low-power passive-dynamic walking mechanism and fly. Such a design is advantageous in a wide range of temporal-spacial applications, where high mobility is required but constant slow movement over long periods of time would place huge energy demands on conventional purely-flying platforms. The design that is proposed is novel and unique

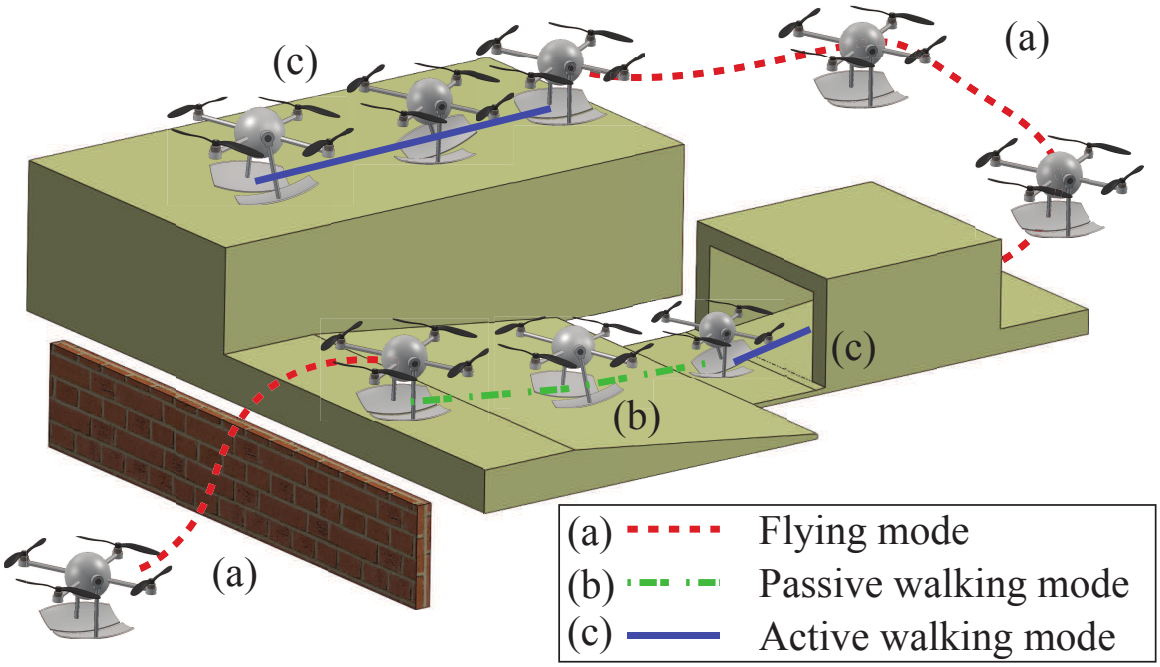

Figure 3.1: The modes of operation for the proposed passive-dynamic flying-walking DUCK robot, showing (a) flying mode, then transitioning to (b) passive walking mode, followed by flying again, and finally, (c) active (powered) mode where the quadcopter's rotors provide the needed force to enable the robot to take steps and walk on flat or up inclined surfaces.

because in addition to flying, it has the ability for passive walking, as well as active or powered walking where the flying platform's rotors can provide small thrust forces to enable the robot to walk on level surfaces as well as up inclined surfaces. This design extends the applicability of passive-dynamic walkers from just traversing down slopes to traversing flat surfaces or up inclined slopes. The combination of passive-dynamic walking with an aerial platform is a new concept.

3.2 Dynamics Modeling

Key features of the DUCK robot are shown in **Figure 3.2**. The robot consists of a hover-capable flying platform connected to passive-dynamic walking legs as shown in **Figure 3.2**(a). The robot has two modes of walking: (1) passive walking down an inclined slope (thrusters turned off) as illustrated in **Figure 3.2**(b) or (2) active (powered) walking where the flying mechanism provides the needed force to enable walking along flat or up inclined surfaces as shown in **Figure 3.2**(c).

The design of the passive-dynamic legs is accomplished by modeling the dynamics of the walking mechanism coupled with the flying platform, then using simulation to tune the parameters of the design. The modeling and simulation adapts details presented in [29–31], where the 3D walking motion is separated into two, 2D models of the lateral (side-to-side) and sagittal (front-to-back) motions as illustrated in **Figure 3.3**(a).

3.2.1 The Equations of Motion

The equations of motion are obtained using the 2D Newton-Euler method, where a dynamic system is modeled as connected rotational or linear joints as depicted in **Figure 3.3**(b) and (c). A recursive process is applied to this model, producing a system of equations that solve for the accelerations of each joint given a starting state. The first step in this process is to create equations for the angular velocities and accelerations of each joint, constructed for $i = 1 \ldots N$, where N denotes the total number of joints. Thus,

$$\vec{\omega}_{i\{i\}} = \mathbf{R}_{i-1,i}\vec{\omega}_{i-1\{i-1\}} + \dot{\theta}_i \hat{r}_{i\{i\}}, \tag{3.1}$$

$$\vec{\dot{\omega}}_{i\{i\}} = \mathbf{R}_{i-1,i}\vec{\dot{\omega}}_{i-1\{i-1\}} + \ddot{\theta}_i \hat{r}_{i\{i\}}, \tag{3.2}$$

where $\vec{\omega}_{i\{i\}}$ and $\vec{\dot{\omega}}_{i\{i\}}$ are the angular velocity and acceleration of joint i relative to the inertial axis, respectively; $\dot{\theta}_i$ and $\ddot{\theta}_i$ are the angular velocity and acceleration scalars of joint

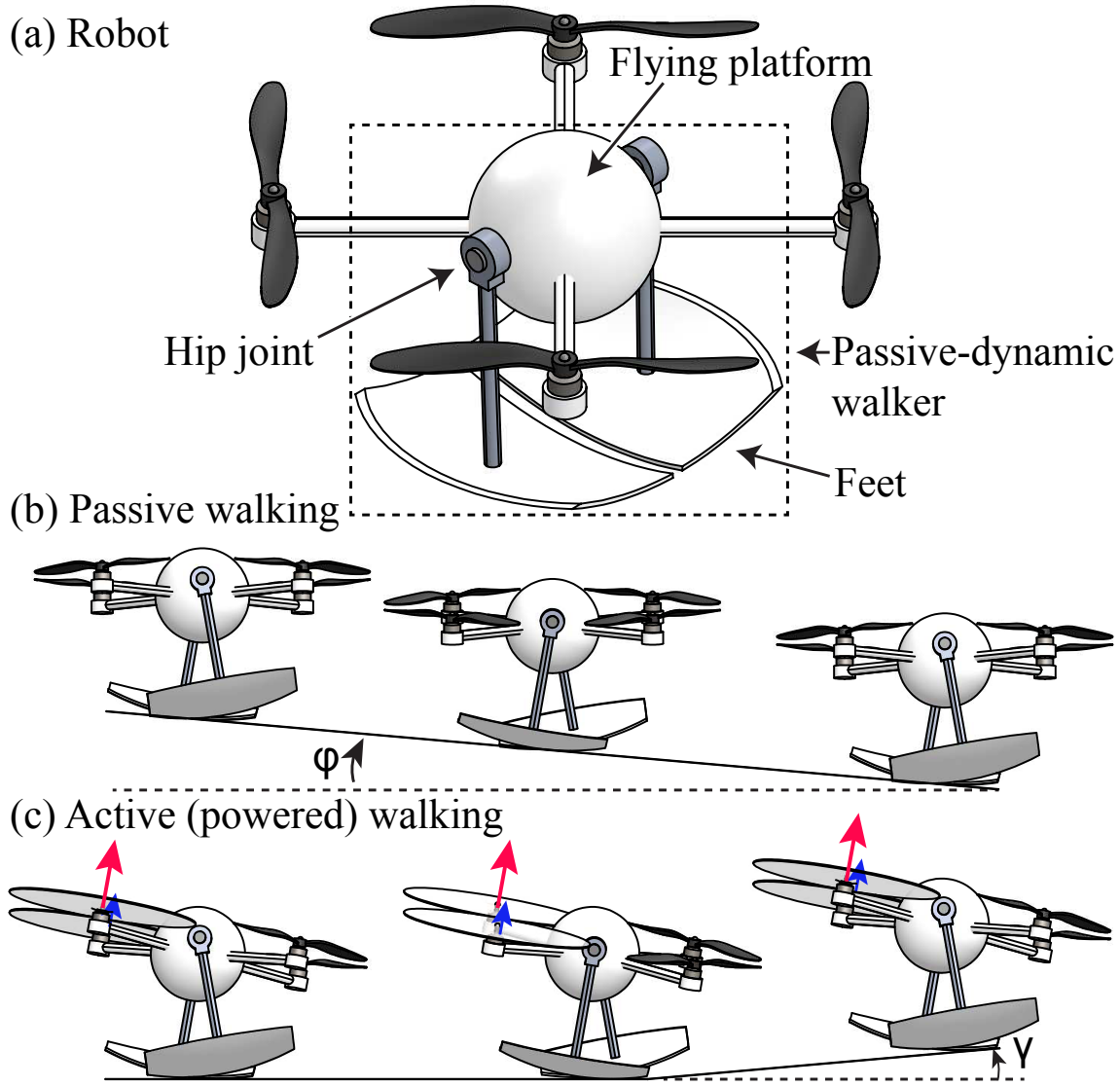

Figure 3.2: Key features of the DUCK robot: (a) key components of the robot, (b) illustration of passive walking without power down a slope of angle ϕ, and (c) illustration of active (powered) walking on flat ground or up a slope of angle γ. During active walking rear thrusters provide forward thrust and rocking motion to enable the robot to take steps and walk.

i relative to the previous joint (measured in radians), respectively; $\mathbf{R}_{m,n}$ is the rotation matrix to change the reference frame of a vector from axes m to axes n; and $\hat{r}_i$ is the rotation axis ($\hat{x}$ for the lateral case and $\hat{y}$ for the sagittal case). For the lateral case $\mathbf{R}_{i-1,i} = [1,0,0,;0,\cos(\theta_i),-\sin(\theta_i);0,\sin(\theta_i),\cos(\theta_i)]$ and $\mathbf{R}_{i-1,i} = [1,0,0;0,\cos(\theta_i),-\sin(\theta_i);0,\sin(\theta_i),\cos(\theta_i)]$ for the sagittal case.

Next, equations for the linear velocities and accelerations of each joint are constructed for $i = 1 \ldots N$, hence

$$\begin{aligned}\dot{\vec{v}}_{i\{i\}} =& \mathbf{R}_{i-1,i}\dot{\vec{v}}_{i-1\{i-1\}} + \ddot{\vec{d}}_{i\{i\}} + 2\vec{\omega}_{i\{i\}} \times \dot{\vec{d}}_{i\{i\}} + \\ & \dot{\vec{\omega}}_{i\{i\}} \times \vec{d}_{i\{i\}} + \vec{\omega}_{i\{i\}} \times (\vec{\omega}_{i\{i\}} \times \vec{d}_{i\{i\}}), \end{aligned} \tag{3.3}$$

$$\begin{aligned}\dot{\vec{v}}_{cg,i\{i\}} =& \dot{\vec{v}}_{i\{i\}} + \dot{\vec{\omega}}_{i\{i\}} \times \vec{d}_{cg,i\{i\}} + \\ & \vec{\omega}_{i\{i\}} \times (\vec{\omega}_{i\{i\}} \times \vec{d}_{cg,i\{i\}}), \end{aligned} \tag{3.4}$$

where $\dot{\vec{v}}_i$ and $\dot{\vec{v}}_{cg,i}$ are the linear accelerations of the i^{th} joint and its center of gravity relative to the inertial frame, respectively; $\vec{d}_i$, $\dot{\vec{d}}_i$, and $\ddot{\vec{d}}_i$ are the linear distance, velocity and acceleration, respectively, from joint $i-1$ to joint i; and $\vec{d}_{cg,i}$ is the linear distance from joint i to its center of gravity. For joint $i = 0$ (the inertial reference frame), $\vec{\omega}_0$, $\dot{\vec{\omega}}_0$, and $\dot{\vec{v}}_0$ are $\vec{0} \triangleq [0;0;0]$.

Next, equations representing the forces and torques on each joint are constructed for $i = N \ldots 1$, thus

$$\begin{aligned}\vec{F}_{i\{i\}} =& \mathbf{R}_{i+1,i}\vec{F}_{i+1\{i+1\}} + m_i\dot{\vec{v}}_{cg,i\{i\}} - m_i\mathbf{R}_{0,i}\vec{g}_{\{0\}} - \\ & \sum \vec{F}_{applied,i\{i\}}, \end{aligned} \tag{3.5}$$

$$\begin{aligned}\vec{u}_{i\{i\}} =& \mathbf{R}_{i+1,i}\vec{u}_{i+1\{i+1\}} - \vec{F}_{i\{i\}} \times (\vec{d}_{i\{i\}} + \vec{d}_{cg,i\{i\}}) + \\ & (\mathbf{R}_{i+1,i}\vec{F}_{i+1\{i+1\}}) \times \vec{d}_{cg,i\{i\}} - \mathbf{I}_i\dot{\vec{\omega}}_{i\{i\}} + \\ & \sum_{n=1}^{m} \vec{F}_{applied,i\{i\}} \times \vec{d}_{\vec{F}_{applied,i\{i\}}} + \vec{u}_{Fric,i\{i\}}, \end{aligned} \tag{3.6}$$

where

$$\mathbf{R}_{i+1,i} = \mathbf{R}_{i,i+1}^T, \tag{3.7}$$

$$\mathbf{R}_{0,i} = \mathbf{R}_{0,1}\mathbf{R}_{1,2}\ldots\mathbf{R}_{i-1,i}, \tag{3.8}$$

$$\mathbf{I}_i = \begin{bmatrix} I_{xi} & 0 & 0 \\ 0 & I_{yi} & 0 \\ 0 & 0 & I_{zi} \end{bmatrix}, \tag{3.9}$$

and $\vec{F}_i$ and $\vec{u}_i$ are the total forces and torques on link i (always $\vec{0}$), respectively; m_i is the mass of link i; $\vec{g}_{\{0\}}$ is the gravity vector ($[0, -g, 0,]$); $\vec{u}_{Fric,i}$ is the torsional friction on joint i; $\mathbf{I}_i$ is the inertial matrix of joint i; and $\vec{F}_{applied,i}$ and $\vec{d}_{\vec{F}_{applied,i}}$ are an applied force on link i and its distance from the center of gravity of link i, respectively. Also, $\vec{F}_{N+1}$ and $\vec{u}_{N+1}$ are $\vec{0}$.

Next, the torques or forces on each joint is extracted for $i = 1 \ldots N$, therefore

$$\begin{aligned} E_{qu,i} &= \hat{l}_{i\{i\}} \bullet \vec{F}_{i\{i\}} \text{ for linear joints,} && (3.10) \\ &= \hat{r}_{i\{i\}} \bullet \vec{u}_{i\{i\}} \text{ for rotational joints,} && (3.11) \end{aligned}$$

where $E_{qu,i}$ is the equation for joint i, and $\hat{l}_i$ is the linear joint's axis ($\hat{y}_i$ for the lateral case and $\hat{x}_i$ for the sagittal case).

Lastly, to make all angles be measured relative to their starting point, and not the previous joint, the following symbolic substitution is made into each $E_{qu,i}$ equation, for $j = N \ldots 1$,

$$\begin{gathered} \theta_j = \theta_j - \Big(\sum_{k=1}^{j-1} \theta_k\Big), \qquad \dot{\theta}_j = \dot{\theta}_j - \Big(\sum_{k=1}^{j-1} \dot{\theta}_k\Big), \\ \ddot{\theta}_j = \ddot{\theta}_j - \Big(\sum_{k=1}^{j-1} \ddot{\theta}_k\Big), \end{gathered} \tag{3.12}$$

where θ_i, $\dot{\theta}_i$, and $\ddot{\theta}_i$ for linear joints are zero. A system of N equations with N unknowns (the acceleration of each joint) is created using $E_i = 0$ for each joint. This system of equations describes the instantaneous motions of the robot given any starting state.

To create a simulation of the DUCK robot's walking behavior, the equations of motion for both the lateral and sagittal movements are needed. The lateral motion equation is obtained with the Newton-Euler method using two joints and the sagittal motion equation requires four joints as shown in **Figure 3.3**. The dimensions of the robot are shown in **Figure 3.4**. Information describing the setup for the lateral motion is provided in **Table 3.1** through **Table 3.3**, while **Table 3.4** through **Table 3.6** describe the sagittal motion. The resulting equation for the lateral motion is given by

$$\begin{aligned} \ddot{\theta}_{2L} =& (2r_L(F_{tot} - m_{tot}a_{cg}\dot{\theta}_{2L}^2) - 2m_{tot}a_{cg}g)\sin(\theta_{2L}) - \\ & w_L(F_{BL} + F_{FL} - F_{BR} - F_{FR}), \end{aligned} \tag{3.13}$$

where F_{BL}, F_{FL}, F_{BR}, F_{FR}, and F_{tot} are the back left, front left, back right, front right, and total thruster forces, respectively; r_L and w_L are the lateral rolling radius and wingspan,

Table 3.1: Newton-Euler joints for the lateral motion

Joint	m_i	I_{xi}	θ_i	$\vec{d}_{i\{i\}}$	$\vec{d}_{cg,i\{i\}}$
0	0	0	0	$\vec{0}$	$\vec{0}$
1	0	0	0	$2\pi r_L \theta_{2L} \hat{y}_{1\{1\}}$	$\vec{0}$
2	m_{tot}	I_{totL}	θ_{2L}	$\vec{0}$	$-a_{cg}\hat{z}_{2\{2\}}$

Table 3.2: Applied thruster and frictional forces for the lateral motion

Force	Joint	Vector	$\vec{d}_{\vec{F}_{applied,i\{i\}}}$
$\vec{F}_{F2L}$	2	$F_{F2L}\mathbf{R}_{1,2}\hat{y}_{1\{1\}}$	$-r_L\mathbf{R}_{1,2}\hat{y}_{1\{1\}}$
$\vec{F}_{L2L}$	2	$(F_{BL}+F_{FL})\hat{z}_{2\{2\}}$	$-0.5w_L\hat{y}_{2\{2\}}$
$\vec{F}_{R2L}$	2	$(F_{BR}+F_{FR})\hat{z}_{2\{2\}}$	$0.5w_L\hat{y}_{2\{2\}}$

Table 3.3: Torsional friction for the lateral motion

Torsion	Joint	Vector
$\vec{u}_{Fric,i\{i\}}$	1, 2, 3	$\vec{0}$

respectively; m_{tot} is the total mass; and a_{cg} is the distance from the lateral center of curvature to the collective center of gravity. The equation for the sagittal motion is found using the same process as for the lateral motion and is omitted for brevity.

Equation 3.13 does not describe the lateral motion while the robot is on the inside edge of its feet ($|\theta_{2L}| < v_{in}$). Adapting details presented in [30] and [29], using $\sum T = I\ddot{\theta}$ to sum torques about the foot's inside edge yields

$$\ddot{\theta}_{2L} = \frac{\sum T}{I}, \tag{3.14}$$

where

$$\begin{aligned}\sum T = \mp\, & m_{tot} g(a_{cg}\sin(\pm\theta_{2L}) + r_L \sin(v_{in} \mp \theta_{2L})) + \\ & (w_L/2 \pm r_L \sin(v_{in}))(F_{BR}+F_{FR}) - \\ & (w_L/2 \mp r_L \sin(v_{in}))(F_{BL}+F_{FL}),\end{aligned} \tag{3.15}$$

$$I = I_{totL} + m_{tot}(a_{cg}^2 + r_L^2 - 2r_L a_{cg}\cos(v_{in})). \tag{3.16}$$

In the above equations, the top signs of "$\mp$" and "$\pm$" are used when the robot is on its left leg, and the bottom signs when on its right leg.

Table 3.4: Newton-Euler joints for the sagittal motion

Joint	m_i	I_{yi}	θ_i	$d_{i\{i\}}$	$\vec{d}_{cg,i\{i\}}$
0	0	0	0	$\vec{0}$	$\vec{0}$
1	0	0	ϕ	$2\pi r_S \theta_{2S} \hat{x}_{1\{1\}}$	$\vec{0}$
2	m_l	I_{lS}	θ_{2S}	$-b_{cg}\hat{z}_{2\{2\}}$	$-b_{cg}\hat{z}_{2\{2\}}$
3	m_q	I_{qS}	θ_{3S}	$\vec{0}$	$-c\hat{z}_{3\{3\}}$
4	m_l	I_{lS}	θ_{4S}	$\vec{0}$	$-b_{cg}\hat{z}_{4\{4\}}$

Table 3.5: Applied thruster and frictional forces for the sagittal motion

Force	Joint	Vector	$\vec{d}_{\vec{F}_{applied,i\{i\}}}$
$\vec{F}_{F2S}$	2	$F_{S2F}\mathbf{R}_{1,2}\hat{x}_{1\{1\}}$	$(r_S - d)\mathbf{R}_{1,2}\hat{z}_{1\{1\}} - b_{cg}\hat{z}_{2\{2\}}$
$\vec{F}_{B3S}$	3	$(F_{BL} + F_{BR})\hat{x}_{3\{3\}}$	$0.5w_S\hat{z}_{3\{3\}}$
$\vec{F}_{F3S}$	3	$(F_{FL} + F_{FR})\hat{x}_{3\{3\}}$	$-0.5w_S\hat{z}_{3\{3\}}$

Table 3.6: Torsional friction for the sagittal motion

Torsion	Joint	Vector
$\vec{u}_{Fric,i\{i\}}$	1, 2	$\vec{0}$
$\vec{u}_{Fric,3\{3\}}$	3	$-.5\mu_b(m_l + m_q)d_b sign(\dot{\theta}_3)\hat{z}$
$\vec{u}_{Fric,4\{4\}}$	4	$-.5\mu_b(m_l + m_q)d_b sign(\dot{\theta}_4)\hat{z}$

3.2.2 Handling Collisions

A collision between the feet and the ground is assumed to occur when the robot transitions between leaning left or right (the angle θ_{2L} changes sign). Collisions in the lateral plane are handled by adapting details presented in [30] and [29]. Here, it is assumed that an inelastic collision occurs between the leg and the ground, thus

$$\dot{\theta}_{2L}^{+} = \dot{\theta}_{2L}^{-} \cos\left[2\tan\left(\frac{r_L \sin(v_{in})}{r_L \cos(v_{in}) - a_{cg}}\right)\right], \tag{3.17}$$

where the superscripts "$-$" and "$+$" mean before and after the collision, respectively. The assumption that the collision is inelastic also assumes a coefficient of restitution of zero for this collision.

In previous works collisions in the sagittal plane were solved using the conservation of angular momentum. This approach is made difficult in this work by the addition of the quadcopter and this technique ignores energy loss due to feet scuffing. This paper takes a new approach to solving these collisions by leveraging the equations of motion

presented above. When there is a transition between which leg is on the ground, if the system's angular velocities are kept the same there will appear to be a discontinuity in the system's momentum. This occurs since the leg describing the system's translational velocity changes. To correct this it is assumed that for one simulation step the robot is sliding with a large frictional force ($\vec{F}_{F2S}$ in **Figure 3.3**). This sliding ends once the system's velocity predicted by Newton's Second Law matches the system's velocity predicted by the Newton-Euler equations of motion. The frictional force which causes this is solved for, and then applied for one simulation step. Only the component of velocity parallel to the slope is considered. To do this first the equation for the center of masses' velocity after an applied frictional force is predicted with Newton's Second Law using

$$v_{fin} = v_{ini} + \frac{F_f}{m_{tot}}\Delta t, \tag{3.18}$$

where v_{ini} and v_{fin} are the components of initial and final velocities of the system's center of mass parallel to the slope, respectively; F_f is the frictional force; and Δt is the duration of one simulation time step. Next, in the Newton-Euler equations which leg's θ, $\dot{\theta}$, and $\ddot{\theta}$ define joints 2 and 4 in **Figure 3.3** is switched, changing which leg is on the ground. Then an equation that finds v_{fin} after a frictional force F_f has been applied to this state is generated. This is set equal to **Equation 3.18** to solve for F_f. Returning to the main simulation, the leg defining the grounded leg is switched, and the frictional force F_f is applied for one time step. The simulation then continues normally.

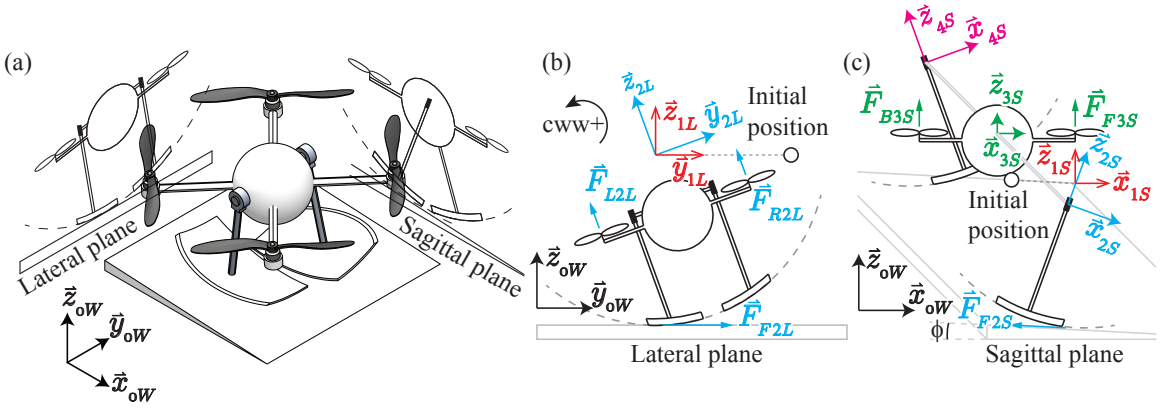

Figure 3.3: Depiction of how the 3D walking motion is split into separate lateral and sagittal motions for modeling [14]–[16]. (a) shows the 3D motion projected onto the 2D lateral and sagittal planes. (b) and (c) are free body diagrams for the lateral and sagittal motions, respectively. Forces ($\vec{F}_{...}$) are determined independently during simulation.

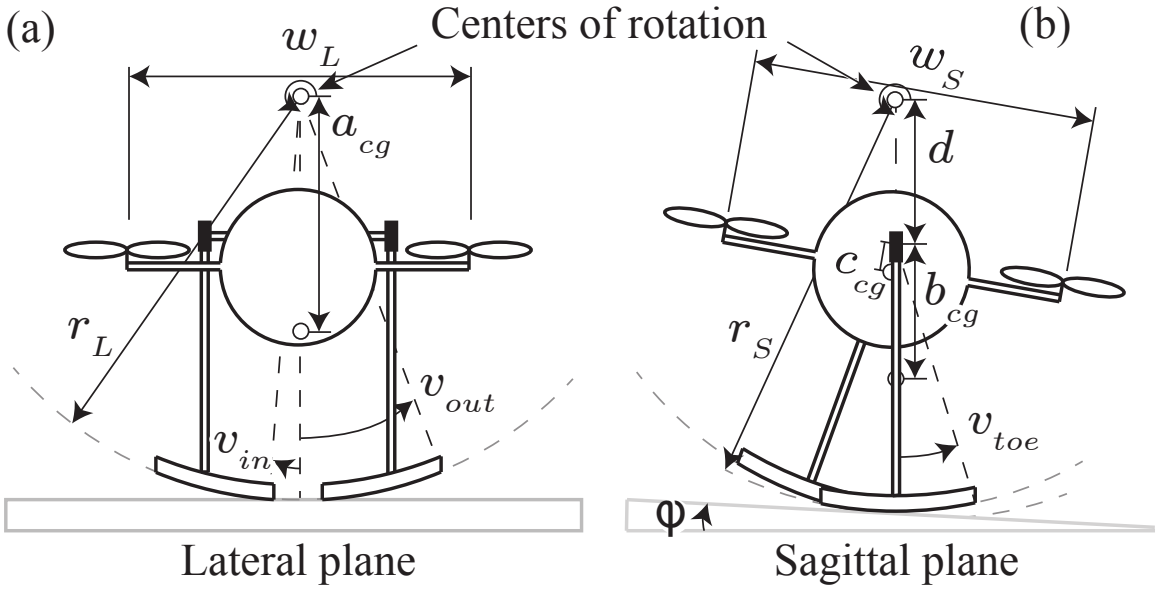

Figure 3.4: Outline of dimensions used in the DUCK robot. (a) The lateral dimensions and (b) the sagittal dimensions.

CHAPTER 4

SIMULATION, DESIGN, AND PROTOTYPE DEVELOPMENT

4.1 DUCK Robot Designs

The two prototype DUCK robots, Version 1 and Version 2, shown in **Figure 1.2** were developed and tested. The mechanical design of the DUCK robot's legs was done using the solid modeling program Solidworks. The fine tuning of the leg's dimensions was done through simulation of the the equations of motion as presented in **Section 3.2**. Unlike many of the previous works in passive walking, to ensure the robot can fly efficiently the mechanical design focuses on weight and size reduction. This leaves the shape of the feet as the only variable which can be used to tune the passive-dynamic walking. However, it was found that the simulated walking could be effectively tuned using only r_L (lateral rolling radius) and r_S (sagittal rolling radius). Tuning was only performed for passive-dynamic walking, as it is harder to achieve than active walking. Initial guesses at the robot's mass properties were provided through weight-accurate SolidWorks models. It was found that r_S needed to be minimized, but not so much that the DUCK robot would fall over while walking ($\theta_{2S} - \phi < v_{toe}$). A large r_S increases the step size, causing the robot to lurch forward during steps. This induces large variations in the leg's sagittal free swinging frequency and makes walking difficult to tune. Next, r_L was used to tune the lateral rocking frequency to the leg's sagittal swinging frequency. The objective was to make the DUCK robot enter a stable limit cycle, such as the one depicted in **Figure 4.1**, from any position starting from rest. A smaller r_L was found to be preferred as it produces a more consistent lateral rocking frequency over a wide range of starting positions. The gap between the feet v_{in} and the distance between the hip's center of rotation and the quadcopter's center of gravity c_{cg} were also both minimized. A small v_{in} minimizes the

energy loss as described by **Equation 3.17**. A small c_{cg} minimizes the effects the swinging quadcopter has on the walking, since the quadcopter's large mass can swing at a different frequency than the legs. A ϕ (slope angle) of -2.3° was used during simulation and tuning.

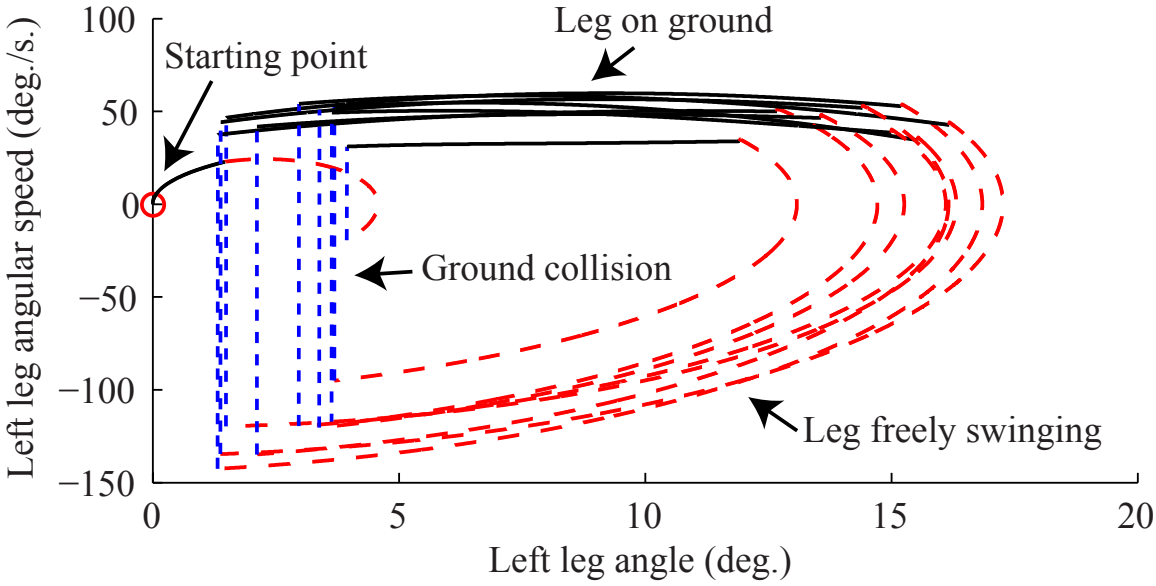

Figure 4.1: Simulated phase portrait for the left leg of Version 1 of the DUCK robot, showing the robot beginning to enter a stable limit cycle. The robot was started from rest standing straight up with θ_{2L} (lateral lean) = 2.3° and ϕ (slope angle) = -2.3°. No thruster forces were used.

It is important to note that in other passive-dynamic walker designs the hip joint is kept at or above the sagittal center of rolling, preventing the swinging foot from unexpectedly colliding with the ground [17, 31]. Due to weight and geometric constraints the DUCK robot doesn't have this in its design. Thus, the simulation's assumption that transitions between legs only happen when θ_{2L} changes sign is not always true. However, a comparison between simulated and experimental data suggests that this was not a major issue.

4.2 Prototype Manufacturing: Version 1

A prototype DUCK robot (Version 1) was created based on the modeling and simulation results. The robot's components and dimensions are shown in **Figure 1.2**(a) and **Figure 4.2**(a) and (b). A commercially available Iris (3D Robotics) quadcopter was used as the flying platform. The passive-dynamic legs consist of a custom-designed hip joint,

lightweight aluminum legs, and 3D printed ABS plastic feet. Each hip joint is made from two cartridge bearings fitted inside an aluminum housing. The dual bearing design increased weight, but was necessary for rigidity which prevented energy loss while walking. The hip and leg shaft were joined via a tolerance fit and clamp. The angle of the foot about the $\hat{z}$ axis was adjusted by rotating the shaft within the feet. This was found to be important for adjusting against imbalances that would cause the DUCK robot to walk sideways, instead of straight down the slope.

4.3 Prototype Manufacturing: Version 2

There was concern about the issues of friction and non-rigidity with the original design, Version 1, from the construction of its hip joints. Each joint on the robot compresses two cartridge bearings in the axial direction in order to achieve a stiff joint (see b) in **Figure 4.2**. However, the bearing's friction and wear increases as this compression force increase. This makes it difficult to make a joint which is both rigid and smooth. Version 2 has a hip bearing which alleviates this problem by not requiring a axial load on its bearings to stiffen the joint. Instead the stiffness of the joint comes from the large distance between the joint's two bearings, and through the use of higher quality bearings. The robot's components and dimensions are shown in **Figure 1.2**(b) and **Figure 4.2**(c) and (d). The retaining clips on the sides of the joints are to prevent the bearings from sliding up or down their axle, though this proved to be unnecessary.

Compared to Version 1, Version 2 is significantly lighter (1.3 kg vs. 1.9 kg) and shorter (15.6 cm vs. 21.2 cm). The leg's hip joint is also significantly more rigid. In Version 1 the slop in the leg joint was enough to be seen by the eye, while the new design has no perceivable slop. Also, the balls in bearings on Version 1 had enough friction at points that the user could be feel them catching on the bearing's rings. Version 2 has higher quality bearings with little to no perceivable friction.

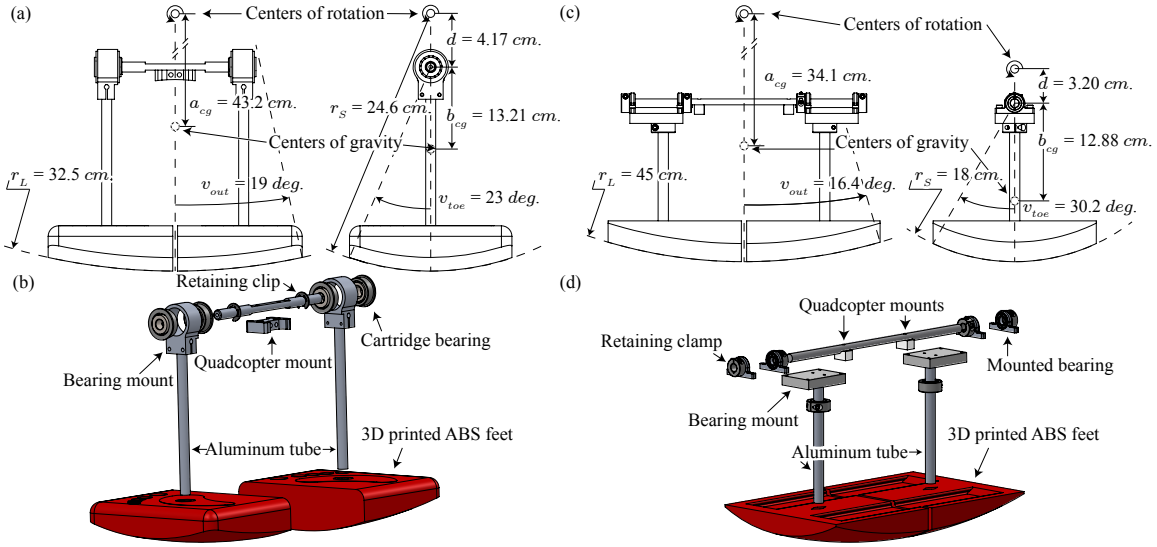

Figure 4.2: Mechanical drawings of the passive-dynamic walking legs, comparing Version 1 (left) and Version 2 (right) designs, where (a) and (c) show the dimensions and (b) and (d) show an exploded view of the mechanism.

CHAPTER 5

PERFORMANCE CHARACTERIZATION AND ENERGY ANALYSIS

5.1 Performance of Version 1 Design

Testing of the DUCK robot and validation of the simulation results were performed using the experimental setup shown in **Figure 5.1**. In the experiment the DUCK robot walked down a sloped treadmill while having its position and pose recorded by a motion capture system (VICON). The VICON system tracks the infrared (IR) markers attached to the robot as shown in **Figure 5.1**. It was found that the DUCK robot was able to maintain a passive walk on slopes with angle between -0.6°and -3.1°. Steeper slopes caused the robot to fall over, and shallower slopes could not sustain a passive-dynamic walk. The DUCK robot's passive walking was limited by oscillations in the walking direction to the left and right which would increase in size until the robot walked off the treadmill, which was probably caused by a lack of frictional dampening in the robot's twisting motion.

The simulation was validated using the motion capture data from the experiments. A time was selected from the experimental data when the DUCK robot's walking had reached steady state, and then this information was used as the initial state in the simulation. The experimental and simulated responses are compared in **Figure 5.2**. The method proposed for handling sagittal collisions as described in **Section 3.2.2** appeared to yield good results, suggested by the good agreement between the experimental and simulated responses. Specifically, the sharp changes in the left leg's angular velocity between transitions measured experimentally matched the simulated behavior. The lateral rocking and sagittal swinging frequencies were predicted to within 9% of the measured frequency. The final amplitudes of the lateral rocking and quadcopter's sagittal swing were predicted to within 12%, but the leg's final sagittal swinging amplitude was predicted to

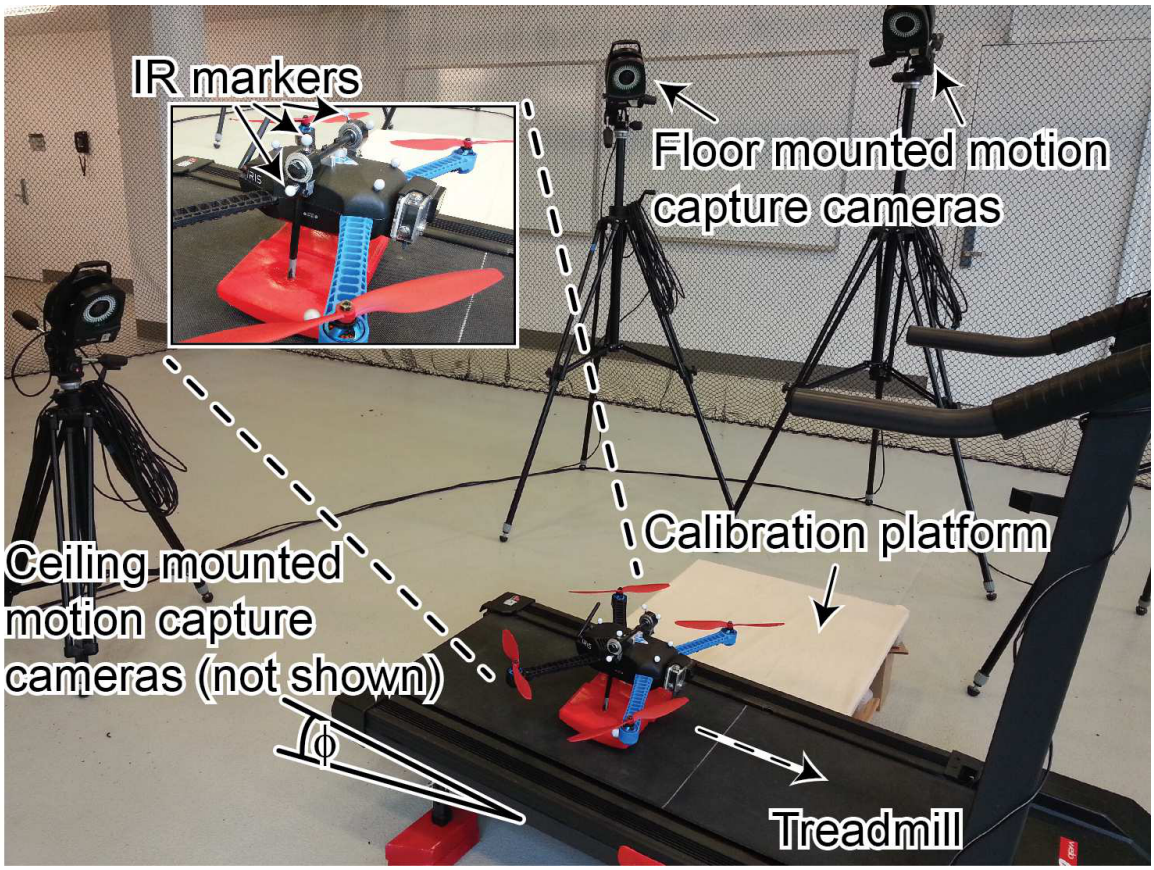

Figure 5.1: Experimental setup for testing passive-dynamic walking. The DUCK robot's position is recorded by a Vicon motion capture system while it walks down the sloped treadmill. Cameras are the Vicon MX F20 and MX T160 series running at 100 Hz, treadmill is a Cadence 70e series. Here ϕ (slope angle) = -2.3°.

be roughly 3.5 times larger than the experimental value. Overall, the simulation yielded a good prediction of the response in terms of overall shape of the angular motion and frequency, but the amplitude of motion was not in good agreement. A possible reason for the observed inconsistencies in the data is the slop in the hip joints as well as their higher than anticipated friction. This possibility is what lead to the creation of Version 2 of the robot.

5.1.1 Active Walking

One of the key contributions of this paper is the demonstration of active walking. In active walking thrust forces from the quadcopter enable the passive-dynamic legs to walk along flat surfaces or up inclined surfaces. This mode of locomotion is desirable

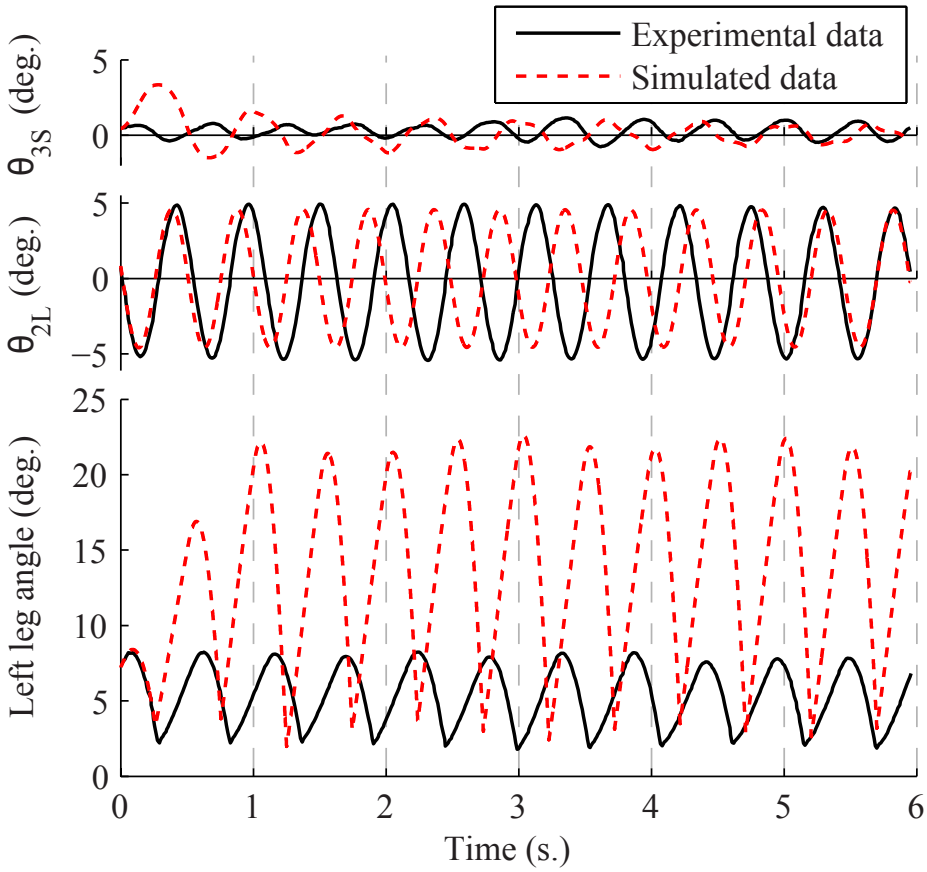

Figure 5.2: Comparison of experimental and simulated results of the robot passively walking. The DUCK robot was allowed to reach a steady walking state on the treadmill shown in **Figure 5.1** while having its position recorded by a motion capture system. An starting point was chosen from this data and used to define the initial state in the simulation. Sagittal quadcopter angle, the angle of joint 3 in **Figure 3.3**(c), is θ_{3S} and lateral lean angle, the angle of joint 2 in **Figure 3.3**(b), is θ_{2L}. Here ϕ (slope angle) is -2.3°.

as it requires less energy in many situations. During tests active walking was achieved through rocking the robot laterally while providing a forward force by rolling and pitching the quadcopter, respectively. As pictured in **Figure 5.3**, under human control the DUCK robot was able to passively walk down a slope, actively walk up a slope, and then fly. Additionally, it was found that during passive walking the quadcopter's stabilization could be turned on, stopping the rocking motions and causing the DUCK robot to stop and wait on the slope. The passive-dynamic walk could be restarted by rolling the quadcopter, then turning off the thrusters. The DUCK robot could be steered left and right by yawing the quadcopter.

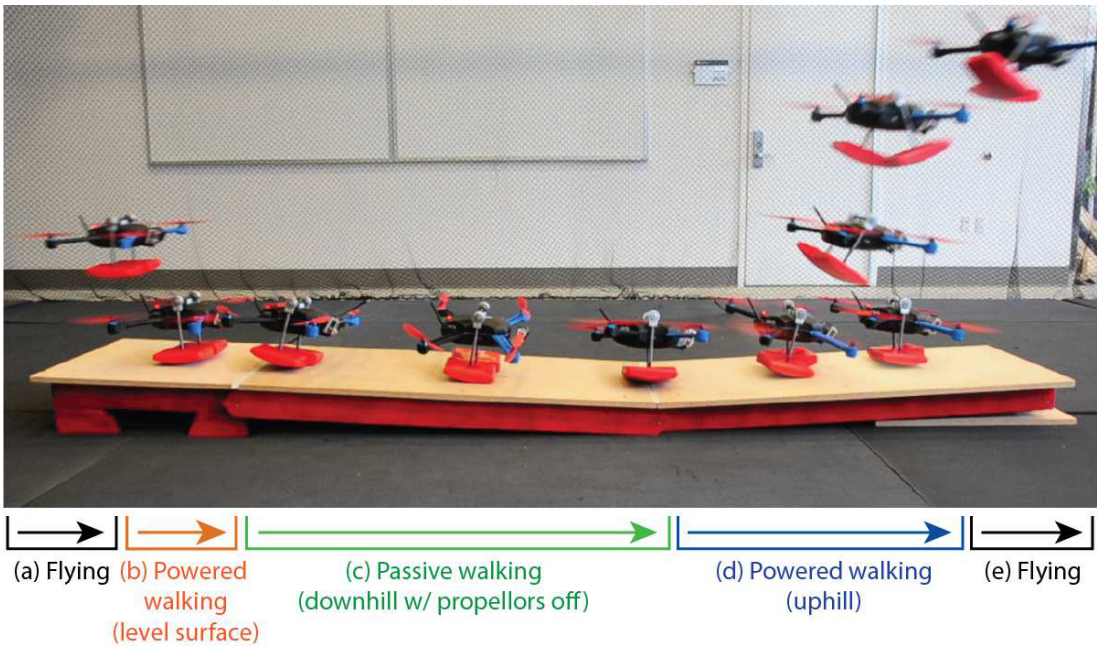

Figure 5.3: Sequence shots of Version 1 of the DUCK robot flying, walking, and then flying again: (a) flying, (b) active (powered) walking on flat surface, (c) passive walking with motors turned off down a -3.1° slope, (d) active walking up a 2.7° slope, and finally (e) take off and flight.

5.1.2 Flying

The added weight and dynamics of the legs affected the quadcopter's ability to fly. Though the quadcopter is still able to fly, the legs would oscillate during flight, requiring additional attitude control. Landing is also made more difficult as the legs were less supportive than a fixed landing gear. It is noted that the internal stabilization of the quadcopter was not altered to account for the weight and dynamics of the legs for all experiments. Future work will consider mechanisms and control algorithms to prevent or minimize swinging of the legs during take-off, landing, and flight.

5.2 Performance of Version 2 Design

Testing of Version 2 of the DUCK robot and a second validation of the simulation results were performed using the experimental setup shown in **Figure 5.4**. This is a copy of the setup used on Version 1. In the experiment the DUCK robot walks down a sloped treadmill while its position and pose are recorded by a motion capture system (VICON). Version 1 had problems during walking tests with oscillations in the walking direction which would

increase in magnitude until the robot fell off the treadmill. Version 2 dose not have this problem. Instead the limiting factor in its walking was its ability to be aimed straight down the treadmill.

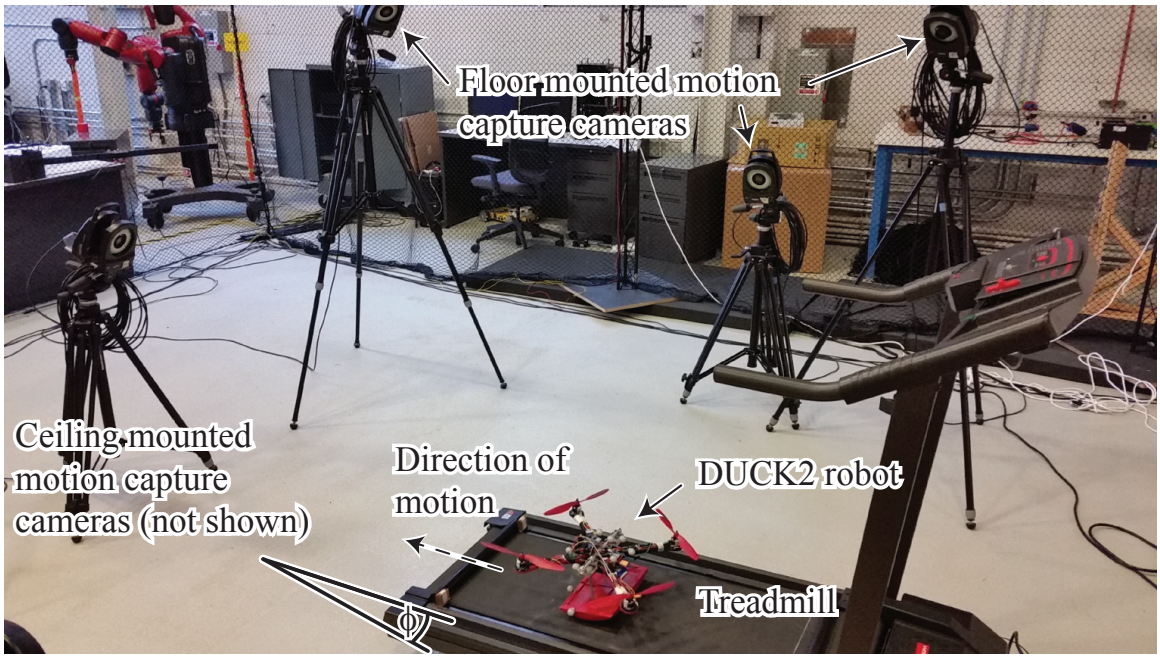

Figure 5.4: Second experimental setup for testing passive-dynamic walking. Like the previous test the DUCK robot's position is recorded by a Vicon motion capture system while it walks down the sloped treadmill. Cameras are the Vicon MX F20 and MX T160 series running at 100 Hz, treadmill is a Cadence 70e series. Here (slope angle) = -2.3.

A second validation of the simulation was done with the same methods used on Version 1 of the robot. A time is selected from the experimental data when the DUCK robot's walking had reached steady state, and then the output of the motion capture data at this time is used as the initial state in the simulation. The experimental and raw simulated responses are compared in (a) on **Figure 5.5**. Like in the previous experiment on Version 1 of the DUCK robot the method described in **Section 3.2.2** to handle collisions appears to yield good results. This is suggested by the similarity between shape changes during collisions in the experimental and simulated data. The amplitudes of the lateral rocking (θ_{2L}) and sagittal quadcopter swing (θ_{3S}) are also predicted correctly. However the lateral rocking frequency is predicted to be about 15% slower that what was shown by experiment (1.7 Hz vs. 2 Hz). This is the opposite of the first experiment, where the lateral

rocking frequency was predicted to be faster than was actually observed. In addition the amplitude of the leg's sagittal swing was predicted to be about three times larger than the observed amplitude. A similar phenomena was observed in the first experiment, however its predicted amplitude was about four times larger than the observed. Its noted that the lateral rocking frequency (θ_{2L}) has a large impact on how the robot walks. To demonstrate how a change in the lateral rocking frequency affects the system a similar experimental comparison was performed, but instead the simulated lateral frequency was altered so that it matched the experimental data. The results of this test are shown in **Figure 5.5**(b). It can be seen that once the simulated lateral frequency matches the experimental, the remaining portions of the experiment begin to have a better match, though there is still a problem in the leg's sagittal swing. This would imply that there are errors in the model of the lateral dynamics, that when fixed would greatly improve the simulation. One possible source of error in both the lateral and sagittal planes is a lack of ways for energy to dissipate in the dynamics model. Having more energy be dissipated would both reduce the lateral rocking frequency and reduce the leg's sagittal swinging amplitude. For instance, the dampening force of friction on both the lateral and sagittal rolling is not modeled. Also, the model is assumed to be perfectly rigid, which ignores the energy losses due to deformations which would happen to the real robot. Its also plausible that the method used for handling collisions in the sagittal plane underestimates the lost energy. However There are areas of the model which overestimate the energy loss of the system. For instance, collisions in the lateral plane are handled by assuming the collision is inelastic, and that the coefficient of restitution is zero. However, in the real world the coefficient of restitution is greater than zero, which would mean the model removes more energy during the collision than it should. Additionally, because the walking motion is modeled as two separate 2D motions, the way in which walking down a slope adds energy to the lateral motions in not modeled. However the dampening effects that the lateral and sagittal motions would have on each other are also not modeled.

5.3 Energy Analysis

An energy analysis is performed to compare the energy efficiency of flying to that of active walking. The energy efficiency of level flight is determined by finding the thrust

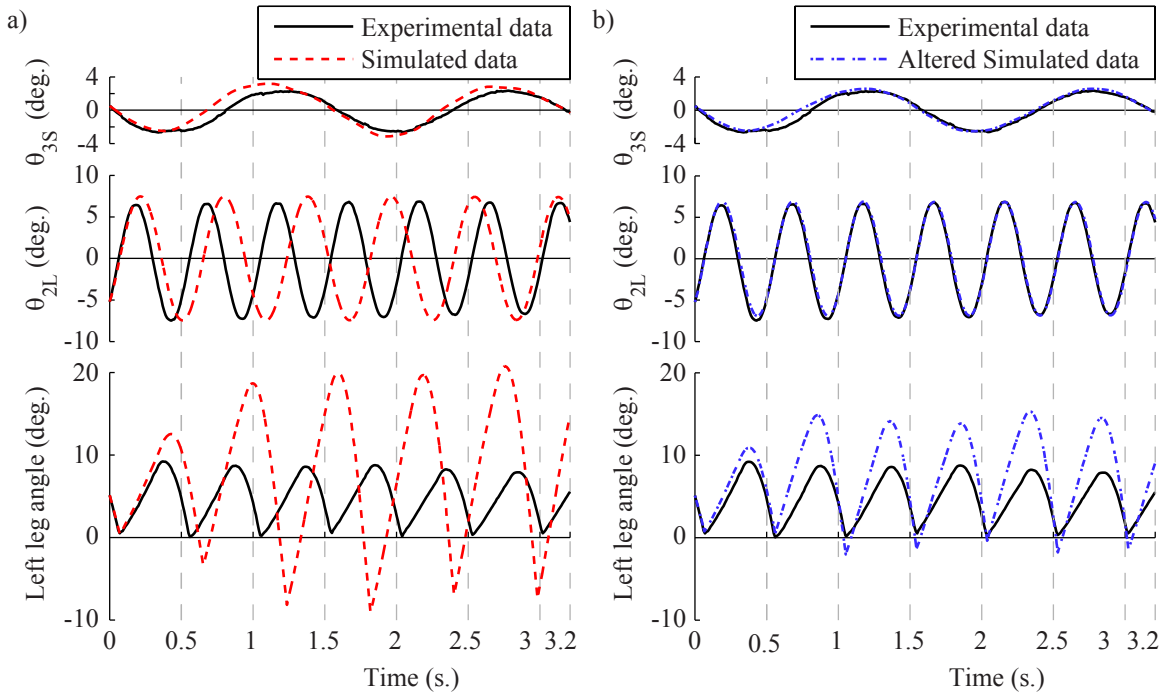

Figure 5.5: Comparison of experimental results of Version 2 of the robot with (a) raw simulated results and (b) altered simulated results, of the DUCK robot's joint angles as it passively walks down a -2.3° slope. In (b) the simulation's lateral moment of inertia was altered so the frequency of the simulated θ_{2L} matched the real data as a demonstration of the system's dependency on the lateral rocking frequency.

force (and implied power) needed to negate air friction and gravity. The energy efficiency of active walking is determined by using the walking simulation described in **Section 3.2** under the effects of various thruster patterns while on a flat surface ($\phi = 0$).

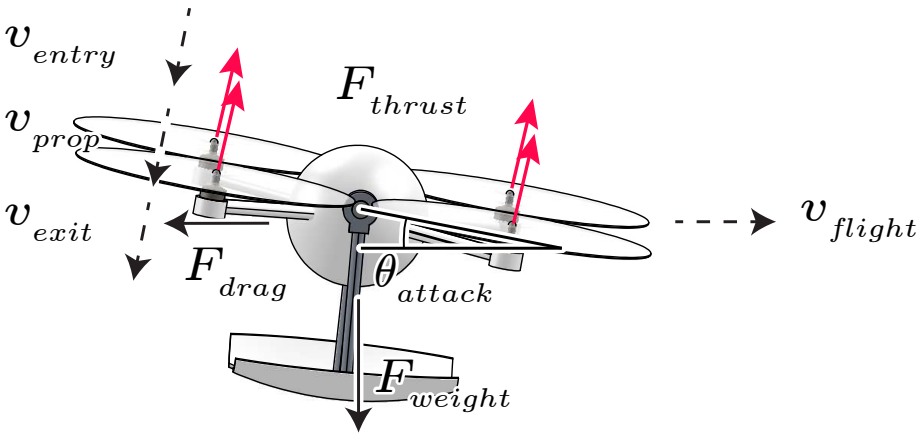

Figure 5.6: Free body diagram of flying. Depicted are the forces and velocities used for calculating the energy efficiency of flying.

To find the energy efficiency of flight the forces shown in **Figure 5.6** need to be determined. The force of drag is estimated by assuming the robot is a 14-cm radius sphere, *i.e.*,

$$F_{drag} = 0.5 c_d \rho \pi r^2 v_{flight}^2, \tag{5.1}$$

$$F_{weight} = mg, \tag{5.2}$$

where F_{drag} is the drag force; c_d is the coefficient of drag for a sphere; r is the radius of the sphere; v_{flight} is the flying velocity; F_{weight} is the force of weight; m is the mass of the robot; and g is the acceleration due to gravity. To maintain a given speed the total thrust of the four propellers needs to counteract the drag and weight forces through the equation

$$F_{total} = 4F_{thrust} = \sqrt{F_{weight}^2 + F_{drag}^2}, \tag{5.3}$$

where F_{total} is the total thrust and F_{thrust} is the thrust provided by one propeller. To estimate the required power to produce a thrust force during flight, actuator disk theory (Momentum Theory) with ideal flow is used, which provides the equations

$$F_{thrust} = \frac{\pi}{4} D^2 \rho v_{prop} (v_{exit} - v_{entry}), \tag{5.4}$$

$$P_{req} = F_{thrust} v_{prop}, \tag{5.5}$$

$$v_{prop} = (v_{entry} + v_{exit})/2, \tag{5.6}$$

where D is the propeller diameter; ρ is the air density; v_{entry}, v_{prop}, and v_{exit} are the velocity of the air entering, at, and exiting the propeller, respectively; and P_{req} is the required power. The velocity of the air entering the propeller is assumed to be the component of the flight velocity perpendicular to the propeller, resulting in

$$v_{entry} = v_{flight} \sin(\theta_{attack}), \tag{5.7}$$

$$\theta_{attack} = \tan^{-1}(F_{weight}/F_{drag}), \tag{5.8}$$

where θ_{attack} is the angle of attack.

The combination of **Equation 5.1** through **Equation 5.8** predicts the power needed for the DUCK robot to fly at a given velocity. Next, the energy efficiency of active walking is determined through simulation. In the simulation a thruster pattern is applied, the first 8 seconds of walking is ignored to allow the robot to reach steady state, and then its average

velocity and power consumption is found over an additional 12 seconds. **Equation 5.4** through **Equation 5.7** are used to convert the thruster forces to power consumption.

The results from the energy analysis on Version 1 of the robot are shown in **Figure 5.8**(a) and **Figure 5.9**(a). **Figure 5.8** compares the maximum theoretical distance the robot could travel on a single battery by flying or walking. It shows that for this design, flying is the most energy efficient, but only at relatively high speeds. At low speeds, flying's energy efficiency approaches zero, and active walking becomes more efficient. At best, flying is between 13-56 percent more efficient than walking, depending on if the weight of the legs is added. **Figure 5.9** compares the cost of transport for flying or walking. The cost of transport for active walking is at best 1.0 while the cost of transport of flying, with or without the legs, is at best .89. Note that real-world inefficiencies in active walking such as uneven ground are not modeled. The most efficient method found for active walking is to elongate and sustain the lateral rocking motion (θ_{2L}) using only the rear thrusters, pitching the quadcopter forward resulting in forward motion. An example of the thruster pattern used to produce this is shown in **Figure 5.7**.

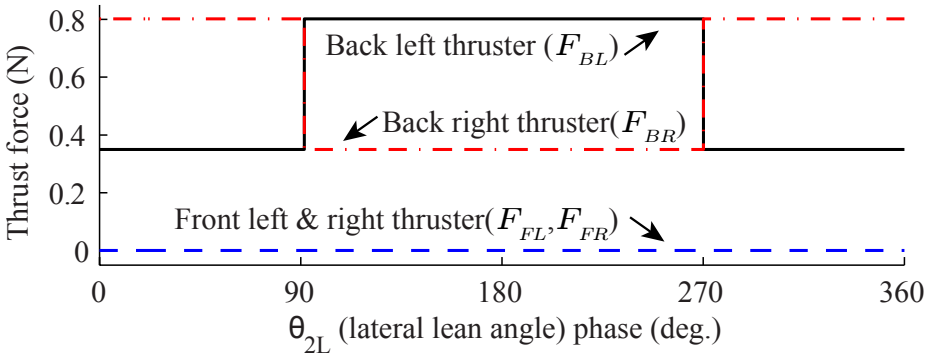

Figure 5.7: Example thruster pattern used for active walking in the simulation. The pattern follows the repetitive motion of θ_{2L}. The rear thrusters are used to provide forward thrust and alter the walking frequency.

A energy analysis for Version 2 of the robot was also performed. The results from this are shown in **Figure 5.8**(b) and **Figure 5.9**(b). It was found that the second design is much more efficient at both flying and walking than the first design, though flying for both versions has the same cost of transport. This is mostly due to the reduced weight of the design, and the increased stability of the legs. In this comparison active walking was

found to be about 7 percent more efficient than flight. Also active walking was found to have a cost of transport of .50 while both modes of flying had a cost of transport of .89.

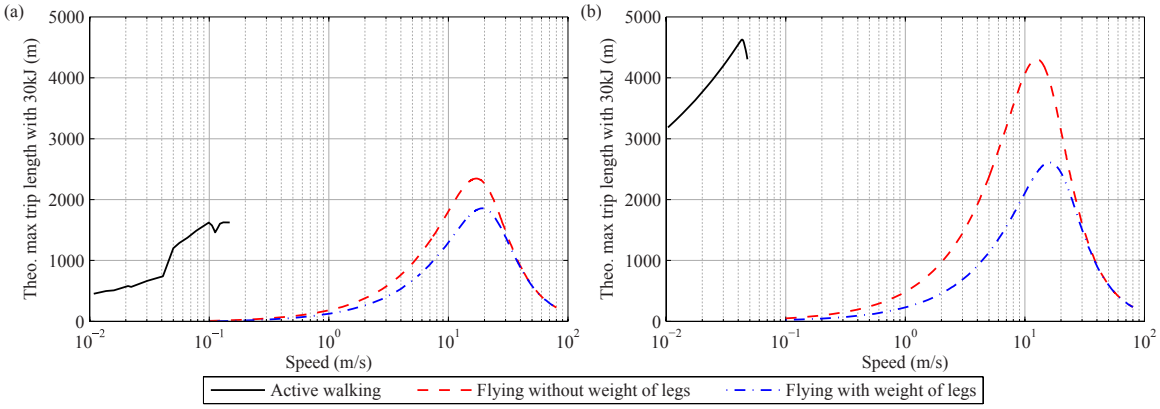

Figure 5.8: Simulation result of estimated maximum distance traveled on 30 kJ (energy in a 2.5 Ah, 11.1 volt battery) v.s. speed for flying and walking. Results for the Version 1 of the DUCK robot are shown in (a), and results for Version 2 are shown in (b). Both version have limits for how fast they can walk without falling over.

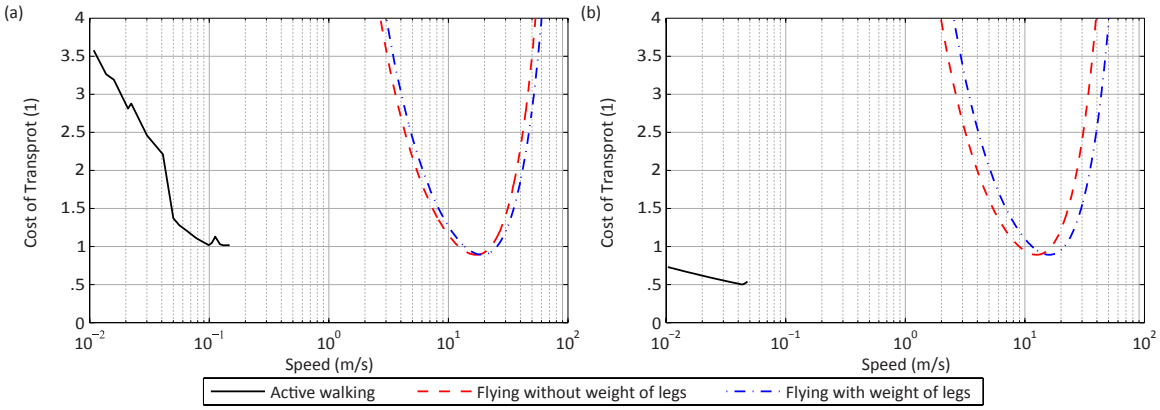

Figure 5.9: Simulation result of the cost of transport for flying and walking. Results for the Version 1 of the DUCK robot are shown in (a), and results for Version 2 are shown in (b). Active walking for Version 1 and 2 has a cost of transport of 1.0 and .50 respectively. Flying has a cost of transport of .89.

Overall it can be observed that some of the discrepancies between the simulated and experimental data in the original experiment were overcome by creating a higher tolerance robot which better matches the assumptions made in the simulation. This presents further evidence for the validation of the simulation used to make the original claims of the theoretical maximum efficiency for active walking and flying. This did not account of all the

errors of the simulation however, which implies un-modeled dynamics are still influencing the system. One hypothesis for the source of this is the un-modeled interactions between the lateral and sagittal motions. Specifically, the affect of the sagittal swinging leg on the lateral motion would most likely increase the frequency of the lateral motion (θ_{2L}) and decrease the amount of energy in the swinging leg, reducing the swing's amplitude. These are the two main discrepancies between the experimental and simulated data.

CHAPTER 6

CONCLUSIONS

This thesis described the development of two walking and flying robots, called the dynamic under-actuated flying-walking robots. The DUCK robots combine a high-mobility quadcopter flying platform with passive-dynamic legs. A detailed mathematical model was presented and the model was used to simulate the walking motion and help design the two prototypes. Two modes of walking were experimentally demonstrated: (1) passive walking down inclined surfaces and (2) active (powered) walking where thrust from the quadcopter's rotors enables the robot to take steps and walk on flat surfaces or up inclined surfaces. The simulation of the walking motion was experimental validated twice using two different designs for the robot. An energy analysis was performed which estimated that on flat ground the robot is more energy efficient at low speeds using active walking, and more efficient at high speeds using flying. For the first design, it is estimated that the robot is able to walk at most 1600 meters on a 30kJ battery (standard Li-Po battery), while the robot can possibly fly at most 1800 meters or 2300 meters with the same battery, with or without the weight of the legs, respectively. The second robot is estimated to be able to walk at most 4600 meters on a 30kJ battery, while it could fly at most 2600 meters or 4300 meters with the same battery, with or without the weight of the legs, respectively. Finally, experimental results demonstrate the feasibility of combining an aerial platform with passive-dynamic legs to create an effective flying and walking robot. In particular, two modes of walking are demonstrated: (1) passive walking down inclined surfaces for low-energy terrestrial locomotion, and (2) active (powered) walking by leveraging the capabilities of the flying platform, where thrust from the quadcopter's rotors enables the DUCK robot to take steps and walk on flat surfaces or up inclined surfaces. Compared to other standard means of ground locomotion such as free-spinning wheels or cages, the DUCK robot has advantages such as being able to stop on sloped surfaces and the ability to

step over small obstacles. However, more research is required before a flying and walking robot like the DUCK robot will have comparable stability and efficiency to that of wheeled aerial-terrestrial robots.

REFERENCES

[1] F. J. Boria, R. J. Bachmann, P. G. Ifju, R. D. Quinn, R. Vaidyanathan, C. Perry, and J. Wagener, *A sensor platform capable of aerial and terrestrial locomotion*, in IEEE/RSJ Int. Conf. on Intelligent Robots and Systems (IROS), Edmonton, Alberta, 2005, pp. 3959–3964.

[2] A. Bozkurt, A. Lal, and R. Gilmour, *Aerial and terrestrial locomotion control of lift assisted insect biobots*, in IEEE Int. Conf. of the Engineering in Medicine and Biology Society (EMBC), IEEE, 2009, pp. 2058–2061.

[3] S. Collins, A. Ruina, R. Tedrake, and M. Wisse, *Efficient bipedal robots based on passive-dynamic walkers*, Science, 307 (2005), pp. 1082–1085.

[4] L. Daler, J. Lecoeur, P. B. Hahlen, and D. Floreano, *A flying robot with adaptive morphology for multi-modal locomotion*, in IEEE/RSJ Int. Conf. on Intelligent Robots and Systems (IROS), Tokyo, 2013, pp. 1361–1366.

[5] L. Daler, S. Mintchev, C. Stefanini, and D. Floreano, *A bioinspired multi-modal flying and walking robot*, Bioinspiration & biomimetics, 10 (2014), p. 016005.

[6] X. Ding and Y. Yu, *Motion planning and stabilization control of a multipropeller multifunction aerial robot*, IEEE/ASME Transactions on Mechatronics, 18 (2013), pp. 645–656.

[7] C. J. Dudley, A. Woods, and K. K. Leang, *Design, fabrication, and modeling of a micro spherical rolling and flying robot*, in IEEE/RSJ Int. Conf. on Intelligent Robots and Systems (IROS), Hamburg, 2015.

[8] M. Elsamanty, M. Fanni, and A. Ramadan, *Novel hybrid ground/aerial autonomous robot*, in First Int. Conf. on Innovative Engineering Systems (ICIES), IEEE, 2012, pp. 103–108.

[9] L. B. Freidovich, U. Mettin, A. S. Shiriaev, and M. W. Spong, *A passive 2-dof walker: Hunting for gaits using virtual holonomic constraints*, IEEE Transactions on Robotics, 25 (2009), pp. 1202–1208. 1552-3098.

[10] A. Goswami, B. Thuilot, and B. Espiau, *Compass-like biped robot part I: Stability and bifurcation of passive gaits*, PhD thesis, INRIA, 1996.

[11] Y. Hanazawa, H. Suda, and M. Yamakita, *Analysis and experiment of flat-footed passive dynamic walker with ankle inerter*, in IEEE Int. Conf. on Robotics and Biomimetics, 2011, pp. 86–91.

[12] K. Hyodo, S. Mikami, T. Narikiyo, and M. Kawanishi, *Turning motion by control constraint mechanism of passive dynamic walking*, in SICE Annual Conference, 2010, pp. 2804–2806.

[13] Y. Ikemata, A. Sano, and H. Fujimoto, *A physical principle of gait generation and its stabilization derived from mechanism of fixed point*, in IEEE Int. Conf. on Robotics and Automation (ICRA), IEEE, 2006, pp. 836–841.

[14] A. Kalantari and M. Spenko, *Design and prototyping of a walking quadrotor*, in ASME International Design Engineering Technical Conferences and Computers and Information in Engineering Conference, Chicago, Illinois, 2012, pp. 1067–1072.

[15] ——, *Design and experimental validation of HyTAQ, a hybrid terrestrial and aerial quadrotor*, in IEEE Int. Conf. on Robotics and Automation, Karlsruhe, 2013, pp. 4445–4450.

[16] K. Kawasaki, M. Zhao, K. Okada, and M. Inaba, *Muwa: Multi-field universal wheel for air-land vehicle with quad variable-pitch propellers*, in IEEE/RSJ Int. Conf. on Intelligent Robots and Systems (IROS), Tokyo, 2013, pp. 1880–1885.

[17] T. Kibayashi, Y. Sugimoto, M. Ishikawa, K. Osuka, and Y. Sankai, *Experiment and analysis of quadrupedal quasi-passive dynamic walking robot "Duke"*, in IEEE/RSJ Int. Conf. on Intelligent Robots and Systems (IROS), Vilamoura, 2012, pp. 299–304.

[18] A. Kossett, R. D'Sa, J. Purvey, and N. Papanikolopoulos, *Design of an improved land/air miniature robot*, in IEEE Int. Conf. on Robotics and Automation (ICRA), Anchorage, Alaska, 2010, pp. 632–637.

[19] J. Li, Y. Tian, X. Huang, H. Chen, and L. Liu, *Torque shaping control for initial unstable passive dynamic walker*, in IEEE Int. Conf. on Information and Automation, 2010, pp. 747–752.

[20] T. McGeer, *Dynamics and control of bipedal locomotion*, Journal of Theoretical Biology, 163 (1993), pp. 277–314.

[21] K. Osuka and K. Kirihara, *Motion analysis and experiments of passive walking robot quartet ii*, in IEEE Int. Conf. on Robotics and Automation, vol. 3, IEEE, 2000, pp. 3052–3056.

[22] D. Owaki, M. Koyama, S. Yamaguchi, S. Kubo, and A. Ishiguro, *A two-dimensional passive dynamic running biped with knees*, in IEEE Int. Conf. on Robotics and Automation (ICRA), 2010, pp. 5237–5242.

[23] K. Peterson, P. Birkmeyer, R. Dudley, and R. S. Fearing, *A wing-assisted running robot and implications for avian flight evolution*, Bioinspiration and Biomimetics, 6 (2011).

[24] K. Peterson and R. S. Fearing, *Experimental dynamics of wing assisted running for a bipedal ornithopter*, in IEEE/RSJ Int. Conf. on Intelligent Robots and Systems (IROS), San Francisco, California, 2011, pp. 5080–5086.

[25] C. Pratt and K. Leang, *Dynamic underactuated flying-walking (duck) robot*, in IEEE Int. Conf. on Robotics and Automation (ICRA), 2016, pp. 3267–3274.

[26] M. Raibert, K. Blankespoor, G. Nelson, and R. Playter, *Bigdog, the rough-terrain quaduped robot*, 2008.

[27] S. Seok, A. Wang, M. Y. Chuah, D. Otten, J. Lang, and S. Kim, *Design principles for highly efficient quadrupeds and implementation on the mit cheetah robot*, in IEEE Int. Conf. on Robotics and Automation (ICRA), IEEE, 2013, pp. 3307–3312.

[28] Y. Sugimoto, H. Yoshioka, and K. Osuka, *Development of super-multi-legged passive dynamic walking robot "jenkka-iii"*, in SICE Annual Conference, 2011, pp. 576–579.

[29] T. Takeguchi, M. Ohashi, and J. Kim, *Toward Human Like Walking-Walking Mechanism of 3D Passive Dynamic Motion with Lateral Rolling-Advances in Human-Robot Interaction*, INTECH Open Access Publisher, 2009.

[30] R. Tedrake, T. W. Zhang, M.-f. Fong, and H. S. Seung, *Actuating a simple 3d passive dynamic walker*, in IEEE Int. Conf. on Robotics and Automation (ICRA), vol. 5, 2004, pp. 4656–4661.

[31] H. Watanabe, S. Fujimoto, and K. Kawamoto, *3D quasi-passive walking of bipedal robot with flat feet-quasi-passive walker driven by antagonistic pneumatic artificial muscle-*, in IEEE Int. Conf. on Advanced Mechatronic Systems (ICAMechS), Tokyo, 2012, pp. 87 – 92.

[32] M. Wisse and J. van Frankenhuyzen, *Design and construction of mike a 2-d autonomous biped based on passive dynamic walking*, in Adaptive Motion of Animals and Machines, H. Kimura, K. Tsuchiya, A. Ishiguro, and H. Witte, eds., Springer Tokyo, Tokyo, 2006, pp. 143–154.

[33] J. W. Yeol and C.-H. Lin, *Development of multi-tentacle micro air vehicle*, in IEEE Int. Conf. on Unmanned Aircraft Systems (ICUAS), Orlando, Flordia, 2014, pp. 815–820.